Formulation Effect on Capsule DPI Performance

The effect of lactose carrier particle size, mixer type, mixing time, and speed

Degree Project in Pharmaceutical Technology, KLGM16 – 30 credits

Author: Maja Tagesson

Supervisor: Kyrre Thalberg

Examiner: Marie Wahlgren

This degree project was performed in collaboration with Emmace Consulting AB, Iconovo, and Magle Chemoswed

Acknowledgments

This master's thesis was conducted at the Department of Process and Life Science Engineering at Lund University in collaboration with Emmace Consulting AB, Iconovo, and Magle Chemoswed.

Firstly, I would like to thank my supervisor, Kyrre Thalberg, for taking time and supporting me during this project, and for all the interesting discussions that have arisen along the way. I would also like to thank Peter Elfman, Jackie Stuckel, and Jonas Jakobsson from Emmace Consulting AB for providing help and guidance during the NGI and SprayTec measurements. Furthermore, I would like to thank Elisabeth Wanngård at Iconovo for spending a day with me at Iconovo to produce batches utilizing the Diosna mixer. I would also like to thank Lars-Erik Briggner at Magle Chemoswed for conducting the TAM analysis on three of the batches produced. Lastly, I would like to thank Marie Wahlgren for taking on the role as my examiner.

I am very grateful for the past 5 years I have spent at Lund University, and this master's thesis marks the end of my education in Chemical Engineering.

Thank you,

Maja Tagesson

Abstract

Inhalation as a method for drug delivery has been employed for more than 2000 years and serves many advantages for diseases in the respiratory tract, like cystic fibrosis and asthma. When administrating the drug directly to the respiratory tract it results in rapid effects and elimination of systemic side effects due to more targeted delivery. Dry powder inhalers (DPI) typically consist of the active pharmaceutical ingredient (API) and carrier particles, lactose. These are mixed in a manner where the API sticks to the surfaces of the carrier particles and, upon inhalation, the API detaches from the carrier particles and can reach the lungs.

This degree project aimed to investigate the effect of using different sizes of lactose carrier particles on DPI performance using a capsule inhaler (RS-01, red button). In total, 18 batches were produced, using budesonide as the API and three different sizes of lactose carrier particles (Lactohale® 100, Lactohale® 206, and Respitose® SV003). The effect of using different mixers (Diosna – high-shear mixer, and Turbula T2C – low-shear mixer), as well as mixing speed and time was also investigated. The concept of mixing energy was used to further compare the mixers. Quality parameters such as homogeneity and poured bulk density were conducted, as well as particle size assessment by using the Next Generation Impactor (NGI).

It was concluded that all batches were homogenous and that the bulk density increased for all batches compared to the pure carriers. For batches produced with the Diosna mixer, dispersion decreased with increased mixing time, and the highest FPF was obtained for batches with SV003 as the carrier. The opposite trend was observed for Turbula batches and the highest FPF was obtained for batches utilizing LH100 as the carrier.

Comparing the two mixers, it was established that the mixing energy theory applies to both the Diosna mixer and the Turbula mixer. However, the mixing energy seems to affect the performances of the formulations differently depending on the type of mixer. It was further concluded that the mass of the lactose carrier particle should be included in the mixing energy equation.

Optimera inhalationsbehandlingen: Så påverkar bärarpartikelstorleken och blandningsprocessen läkemedelsprestandan

Inhalering har använts som en metod för administrering av läkemedel i över 2000 år och har många fördelar mot lungsjukdomar som exempelvis cystisk fibros och astma. Lungorna är avgörande för vår andningsfunktion och ansvarar för gasutbytet mellan luft och blod. Genom att leverera läkemedlet direkt till lungorna undviker man biverkningar jämfört med orala läkemedel. För att ta fram läkemedel riktat mot lungorna krävs utveckling av formuleringen av inhalationsläkemedlet. Denna studie undersökte hur olika storlekar på bärarpartiklar i torrpulverinhalatorer påverkar läkemedlets prestanda.

För att tillverka ett torrpulver krävs endast två olika ingredienser; bärarpartiklar och den aktiva substansen. Bärarpartiklarna är mycket större än den aktiva substansen, cirka 50 gånger större. Oftast används laktos som bärarpartikel eftersom det är tillgängligt, billigt och säkert ur ett patientperspektiv. Syftet med att använda bärarpartiklar är att öka flytet på formuleringen. Detta kan liknas vid att hälla strösocker och florsocker från en matsked. Strösockret, som har större sockerpartiklar, kommer lätt att rinna av skeden. Florsockret, som är mer finfördelat, kommer inte rinna av skeden lika lätt som strösockret. Den aktiva substansen finfördelas vanligtvis så att partiklarna blir så små som möjligt. Detta är nödvändigt eftersom partiklarna inte kan nå lungorna om de är för stora. Partiklarna bör vara mindre än 5 mikrometer för bäst upptag långt ner i lungorna.

Det har tidigare gjorts studier kring hur olika laktospartiklar påverkar prestandan av torrpulvret. Däremot är resultaten kring detta ämne förvirrande. Det finns idag inte någon universell teori för hur bärarpartiklarnas storlek påverkar upptagningsförmågan av läkemedlet och därför är detta område intressant. Baserat på dessa kunskapsbrister utfördes detta examensarbete med syfte att undersöka hur storleken på laktosbärarna påverkar prestandan av formuleringen. Blandningstid, blandningshastighet och två olika typer av blandare undersöktes också, en med mer aggressiv blandningsprocess och en med en mildare blandningsprocess.

Resultatet visade att formuleringarna som blandats i blandaren med mer aggressiv blandningsrörelse samt med de minsta laktosbärarna hade större kapacitet att få den aktiva substansen att nå längre ner i lungorna. Den motsatta trenden observerades för formuleringar som producerats med blandaren med mildare blandningsprocess, där den största bärarpartikeln hade störst kapacitet att få den aktiva substansen att nå lungorna.

Det visade sig också att båda blandarna är beroende av den så kallade blandningsenergin men att den påverkar formuleringarna olika beroende på vilken blandare som används. Blandningsenergin är den energi som partiklarna i formuleringen utsätts för under blandning. Denna är beroende av bland annat blandningshastigheten, blandningstiden och massan på en enstaka bärarpartikel.

Table of Contents

1. Introduction

Inhalation as a method for drug delivery has been employed for more than 2000 years and serves many advantages for diseases in the respiratory tract, like cystic fibrosis, asthma, and many more. When administrating the drug directly to the respiratory tract it can result in rapid effects and elimination of systemic side effects due to more targeted delivery. It is also possible to administer a lower dose to achieve therapeutic effects compared to orally administered drugs, also resulting in a lower risk of systemic side effects. The respiratory tract possesses low enzymatic activity, resulting in avoidance of the degradation of drug particles before absorption. [1, 2] It can also be useful to deliver a drug via the pulmonary route, particularly when the drug has limited oral absorption and to avoid first-pass metabolism in the liver. However, the lungs possess their own metabolic capabilities. [3]

The lungs serve as the fundamental organs of the respiratory system, primarily responsible for enabling the exchange of gases between the environment and the bloodstream. Oxygen is transported through the airways to the alveoli and enters the bloodstream. [4] The airways are divided into the upper respiratory tract (nose, throat, thorax, pharynx, and larynx) and the lower respiratory tract (trachea, bronchi, bronchioles, and the alveolar regions). The trachea is divided into two main bronchi, which are further divided into terminal bronchioles, see Figure 1. The terminal bronchioles divide to produce respiratory bronchioles which ultimately leads to the alveolar sacs, consisting of approximately 20-60 billion alveoli and a surface area of about 80 square meters in an adult male. [3]

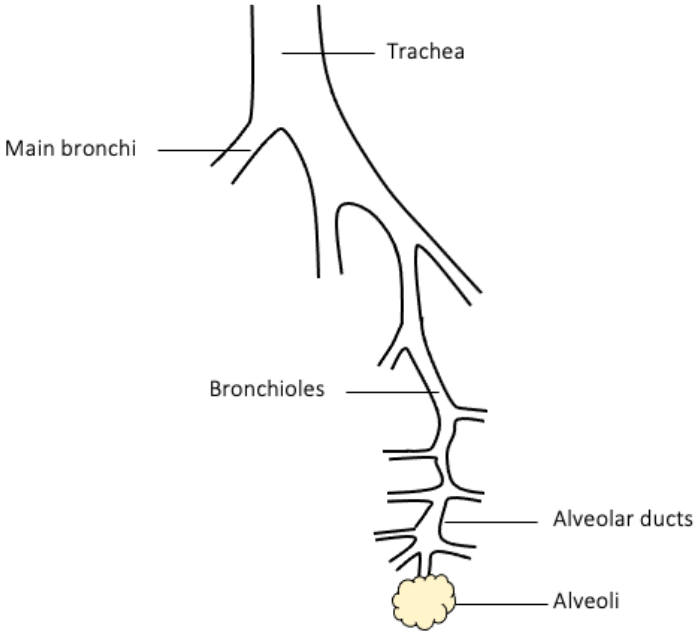

Figure 1: Simplified visual representation of the human airways. Figure adapted from [3].

There are today three main pulmonary drug devices being used; pressurized metered-dose inhalers (pMDIs), dry powder inhalers (DPIs), and nebulizers. Within pMDIs, the medication is incorporated into liquid propellants along with additional excipients. This mixture is contained in a pressurized canister equipped with a metering valve. Upon actuation of the metering valve, a predetermined dose is released as a spray which results in a gas and liquid

mixture before discharge from the orifice. In DPIs, the drug is inhaled in the form of a fine particle cloud. The drug can be preloaded in a device or contained within capsules or foil blister discs, which are loaded into the device before usage. When a drug cannot be formulated in pMDIs or DPIs, it is formulated into a nebulizer. Nebulizers deliver large volumes of drug solutions/suspensions and can be inhaled by normal breathing through, for example, a face mask which enables easy management for small children or the elderly. [3]

The formulation technology regarding pulmonary drug delivery addresses challenges for aerosol dispersion, as well as the fact that the lungs have a lower buffering capacity compared to, for example, the gastrointestinal tract. Furthermore, there is a reduced number of excipients that can be used for enhanced delivery outcomes. [5]

1.1 Aim

The master thesis aims to investigate the impact of lactose carrier size, mixer type, mixing time, and mixing speed on the performance of dry powder inhaler formulations in a capsule inhaler, using budesonide as the API. The mixers that will be used are a low-shear (Turbula T2C) and a high-shear (Diosna), and the mixing speed will differ between the formulations. In total, 18 batches will be produced using three different lactose carriers; Lactohale® 100, Lactohale® 206, and Respitose® SV003, and their performance will be evaluated to understand how these parameters affect the dispersion and aerosolization properties of the DPI formulations. Furthermore, the concept of mixing energy will be used to compare the two mixers.

2. Theory

2.1 Particle deposition

To efficiently deliver a drug via the respiratory tract, the drug must be presented as an aerosol. An aerosol is a system where particles or droplets are dispersed in a gas small enough in size to exhibit significant stability when suspended. The physiochemical properties of the drug, the formulation, the device, and the patient in terms of breathing pattern are all important factors for the deposition of the aerosol in the respiratory tract. [3]

There are three main mechanisms for the deposition of particles in the respiratory tract: gravitational sedimentation, inertial impaction, and brownian diffusion. Inertial impaction comes into play when the aerosolized particles encounter surfaces in the respiratory tract that force changes in direction. Particles with high momentum will impact the airway walls instead of following the changing airstream. The mechanism is common in the upper airways and crucial for particles with a diameter greater than 5 μm. [3]

Gravitational sedimentation is a mechanism of particle deposition that occurs due to the force of gravity acting on aerosol particles and can be described with Stoke's law. The mechanism is particularly important for particles between 0.5-3 μm within the small airways and alveoli, especially for those that have escaped impaction. [3]

Brownian motions are produced by collisions of small particles in the respiratory tract. Particles moving from high to low concentrations result in movements from the aerosol to the airway walls. Brownian diffusion is crucial for particle deposition of very small particles (<0.5 μm) and the diffusion rate is inversely proportional to the particle size. [3]

Other factors that may affect the deposition of the aerosol particles are patient-specific breathing patterns. Greater peripheral distribution of particles in the lung occurs with larger inhaled volumes. Conversely, increasing the inhalation flow rate enhances deposition on the larger airways through inertial impaction. Breath-holding after inhalation boosts particle deposition via sedimentation and diffusion. [3]

2.2 Dry powder inhalers (DPI)

Dry powder inhalers (DPIs) are inhaled as an aerosol and the drug can be loaded in an inhalation device, capsules, blisters, etc., which are loaded in the device before use. Unlike pressurized metered-dose inhalers (pMDIs), DPIs do not require propellants and rely on the patient's inhalation effort to disperse and deliver the drug. Furthermore, DPIs are breath-actuated which eliminates the need to coordinate the inhalation by pressing a button or triggering any other type of mechanism to release the drug. However, DPIs are reliant on the patient's inhalation effort, which can be problematic for certain patient groups (elderly, children, etc.). Moreover, DPIs are exposed to atmospheric conditions which may influence formulation stability in the case of humidity changes that can cause the formulation to form lumps. [3]

DPIs are formulated, as the name indicates, as a dry powder, with an active pharmaceutical ingredient (API) and a carrier (usually lactose). However, it can be formulated with the API alone, or a combination of API and lactose co-spherized. [6]

Lactose is commonly used as an excipient in DPIs due to its availability, low cost, and its well-developed safety profiles. [7] To produce particles with a diameter of less than 5 μm, the drug powder is usually micronized or spray dried. The powders produced have poor flowability due to their cohesive and adhesive nature. The flowability of the powder is dependent on several physical factors including particle size and shape, moisture content, bulk density, surface roughness, and hardness. [3]

2.2.1 Adhesive mixtures

Adhesive mixtures, as previously mentioned, consist of a micronized API and an inert carrier particle. The micronized API and the lactose carriers are mixed in a manner where the API is attached to the surfaces of the carriers, see Figure 2. Adhesive mixtures can also consist of a coating agent, usually magnesium stearate in DPIs, and smaller lactose particles, so-called fines. The purpose of a coating agent is to increase the dispersibility of the drug by reducing surface energies and friction. The purpose of lactose fines is also to improve dispersibility. [8]

Figure 2: Schematic representation of lactose carrier particles and micronized API particles that, upon mixing, will create an adhesive mixture by which the finer API particles attach to the surfaces of the carrier particles. Figure adapted from [9].

2.2.2 Interparticle forces

The powder should be able to withstand mechanical processes, like handling and filling, while being easily separable into the API and carrier during aerosolization (see Figure 3). The homogeneity and aerosolization performance are hence highly dependent on the appropriate balance between drug-drug cohesive forces and drug-carrier adhesive forces. Strong adhesion forces, are beneficial for creating a stable, homogenous mixture, but need to be weak enough to allow for drug-carrier detachment during aerosolization. [10]

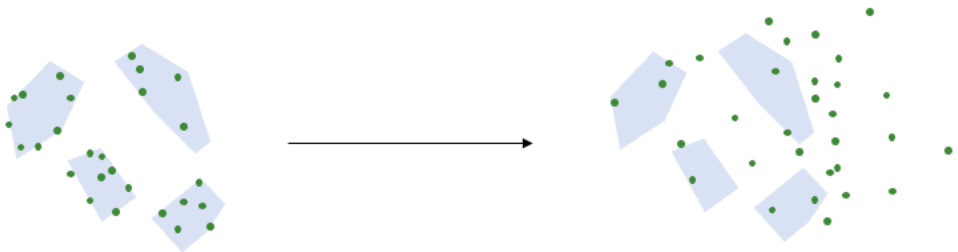

Figure 3: Schematic representation of an adhesive mixture that consists of lactose carrier particles and finer API particles. Upon inhalation, the finer API particles detach from the lactose carrier particles and disperse in the inhaled airstream to reach the lungs. Figure adapted from [8].

Four primary forces govern particle interaction: Van der Waals, capillary forces, electrostatic forces, and mechanical interlock. [5] Van der Waals forces are dominant in situations where particles can dissipate surplus electric charge. Mechanical interlock comes into play when drug particles fit into cavities upon close contact with the surface of the carriers. Electrostatic forces arise when materials with different surface charges come into contact and subsequently separate. Furthermore, capillary forces are generated by the formation of a liquid bridge between particles, a phenomenon influenced by the surrounding relative humidity. The generation of the forces mentioned is further dependent on environmental conditions and properties related to the particles like surface properties, size, and area size. [11]

2.2.3 Aerodynamic particle size distribution

The particle size distribution of an aerosol is a critical physical property as it determines how deeply the drug is carried down the respiratory tract. Typically, the particle size of an aerosol is standardized by the aerodynamic particle diameter (d_a). The definition of d_a is the physical diameter of a unit-density sphere that settles through the air at the same velocity as the specific particle in question. The aerodynamic diameter (for spherical particles) can be described with equation (1):

$$d_a = d_p(\rho/\rho_0)^{1/2} \quad (1)$$

where d_p is defined as the physical diameter, ρ is the particle density and ρ_0 is defined as the density of a unit sphere ($1 g/cm^3$). When using the mass median diameter (MMD) for d_p, d_a is referred to as the mass median aerodynamic diameter (MMAD). [3] The optimal particle size of aerosols has been investigated for different disease states in several studies, and the conclusion is that the optimal particle size varies between 1 and 5 µm. [5]

2.2.4 Cascade Impactors

The most efficient way of measuring the aerodynamic particle size distribution is by using cascade impactors. The general principle of cascade impactors is that the aerosol is drawn through the impactor with a controlled airflow. The aerosol passes through a series of stages. Each impactor stage is designed with a cut-off diameter, representing the size at which particles efficiently deposit. Larger particles will impact in earlier stages, and smaller particles progress to later stages. The inlet to the impactor typically features a 90-degree angle, therefore also called a throat. When the measurement has run, the impactor is disassembled and particles deposited at each stage are analyzed by using, for example, HPLC. [3]

There is a risk that the particles will bounce between the stages, resulting in particles that re-enter the airstream. The bouncing will lead to inaccuracies in particle size distribution determination. [12]

There are two main types of impactors used today: Andersen cascade impactor (ACI) and Next generation impactor (NGI). ACI typically consists of eight stages, with metal collection plates followed by a terminal filter, and is suitable for DPIs and pMDIs. Next generation impactors have seven stages and are intended to operate at a flow rate between 30 l/min and 100 l/min. The particles that are analyzed are collected in cups on a tray, which enables easy handling [13, 14]. To aid drug recovery, one can add suitable solvent directly to the cups. An additional feature is the incorporation of a micro-orifice collector (MOC), designed to capture ultra-fine particles that are typically trapped on the final filter in traditional impactors, and deposit them into a separate collection cup. Subsequently, the particles are analyzed in the same manner as the particles collected at the other stages of the impactor. [13]

2.2.5 Fine particle fraction (FPF)

The fine particle fraction (FPF) can be described as the proportion or percentage of drug particles in an aerosol cloud that is sufficiently small to enter the lungs and induce a therapeutic effect. [15] The FPF is usually described as the percentage of the emitted aerosol that falls within the fine particle size range (usually less than 5 μm). It is desirable to achieve high FPF values when formulating dry powder inhalers as this indicates that a large amount of the drug is delivered to the targeted regions of the respiratory system where absorption and therapeutic effects are maximized. In systems where the concentration of API is low, the FPF value is also low which will result in high dose variations. Moreover, a more appropriate API concentration ranges between 2-15% to achieve higher FPF values. However, higher drug loads than 15% can lead to failure of FPF. Furthermore, it is established that processing conditions (such as the mixing process) influence FPF. [16]

Another key parameter correlated to the FPF is the fine particle dose (FPD), which is defined as the amount of drug particles that can reach the lungs and have an aerodynamic particle size diameter less than 5 μm. [8]

2.2.6 SprayTec

The SpayTec instrument is designed for measuring particle sizes within sprays. Additionally, the emptying time of capsules when used with a capsule inhaler can be measured. It accomplishes this by assessing the distribution of various sizes present in the spray. The measurement process entails several steps, and the first is to prepare the spray and administer it through a suitable delivery device. Moreover, the spray is directed between two key functional components of the instrument, the transmitter and receiver. The transmitter employs a Helium-Neon laser to generate a laser beam, which crosses through the spray delivered to the measurement zone. In the receiver module, detecting optics capture the light diffraction pattern generated by the spray. The captured light is then transformed into electronic signals. Finally, the light diffraction pattern is analyzed utilizing an appropriate scattering model, generating the spray's size distribution. [17]

Particle size distribution with SprayTec assumes that particles are perfect spheres, even though they rarely are in practice. This approach is referred to as equivalent sphere distribution. SprayTec measures size based on volume. However, there are other methods available. For example, one can calculate the diameter of a theoretical sphere with the same surface area as

the original particle (known as the equivalent surface area method). Depending on the method used, the results will vary. However, it is important to use the same method through all the measurements to obtain comparable results. [17]

2.2.7 Carrier design

As mentioned previously, lactose is a commonly used carrier between sizes of 50-200 μm. The primary roles of lactose in a DPI are to enhance flowability (ensuring accurate filling and dosing of the inhaler), facilitate the dispersion of API into inhalable aerosols upon inhalation, and minimize the potential of particle segregation. [18] There are two different kinds of lactose carriers, in terms of shape: single crystal carriers with a "tomahawk" shape, and aggregated crystal carriers. In both categories, the surfaces exhibit irregularities at the nano-and micro-scales. Additional challenges include surfaces of the lactose that may be contaminated by protein residues, fines, or other unwanted material. [8]

The physicochemical properties of the powder highly influence the performance of the DPI. These properties are for example moisture content, particle size and shape, and interparticle forces. [19] Particle shape has a major influence on aerosolization and lung deposition, and it has been determined that adhesion and blend homogeneity are correlated to the surface roughness of the lactose carriers. Additionally, a linear correlation has been confirmed between FPF and surface roughness, suggesting the necessity of some degree of surface roughness to facilitate drug adhesion and blend uniformity. However, excessive roughness may hinder drug release after inhalation, and thus, a lower FPF. [20]

A study investigated the effects of different sizes of lactose carriers and found that smaller lactose carriers correlated with lower adhesion properties between budesonide (API) and lactose. The aerodynamic diameter was also reduced when using smaller lactose carriers, leading to higher budesonide delivery to the lower stages of the impactor, indicating enhanced performance in DPI aerosolization. Furthermore, it was established that the utilization of lactose particles with a smaller aerodynamic diameter adversely affected the homogeneity of budesonide content and resulted in an increased deposition of budesonide in the oropharyngeal region (the part of the throat that includes both the oral cavity and the pharynx). [21]

The impact of carrier particle size has undergone extensive investigation; however, experimental results are frequently perplexing. Currently, there is no universally established theory regarding how carrier particle size influences the fine particle fraction. However, it is established that larger lactose carriers exhibit improved flowability, due to less cohesion, and lower specific surface area, imposing constraints on the drug loading capacity. [8]

2.2.8 Bulk density

Bulk density is determined by the mass (M) of the powder occupying a specific volume (V), see equation (2):

$$\rho_B = \frac{M}{V}\ kgm^{-3} \tag{2}$$

The powder's bulk density serves as a measure of its flowability, varying based on particle packing, and changes as the powder consolidates. Comparing the initial (poured) and final (tapped) bulk densities provides insights into flowability. The Hausner ratio, representing the relationship between tapped and poured bulk density, serves as a valuable tool for predicting powder flow characteristics. [3]

An increase in bulk density results in reduced porosity. As a result, the adhesion and cohesion between the particles increases. For larger particles, these effects may not be significant enough to overcome other factors influencing flow quality. In other words, even with increased adhesion and cohesion due to higher bulk density, larger particles may still show good flowability. Conversely, a decrease in bulk density might result from smaller particle sizes, leading to a loosely packed powder bed. However, despite its porosity, the powder may still exhibit poor flow due to the cohesion between the particles. Figure 4 describes how the bulk density is dependent on the packing geometry. [3]

Due to interparticle pores that are filled with air, the bulk density can never exceed the true density of its component particles. Furthermore, the powder can have many different bulk densities but only one true density, depending on the packing of the particles and the porosity. [3]

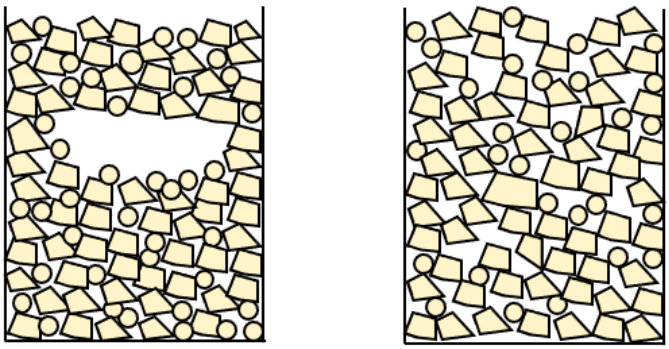

Figure 4: Schematic representation of two powders with the same dimension, sharing equal bulk density but differing in packing geometry. Figure adapted from [3].

2.3 Mixing

The mixing process aims to disperse drug-drug agglomerates and facilitate the even distribution or adhesion of the API onto the surfaces of the carrier particles. [10] The conditions during mixing also influence the interparticle forces, which play a crucial role in determining the FPF. Furthermore, different DPIs may have different mixing requirements due to the existing forces between particles. [5] During mixing, an initial disorder in the powder bed arises. A stabilized blend is achieved when the mixture reaches its maximum stability. Insufficient mixing results in issues regarding dose uniformity. [22]

There are two primary methods for mixing DPIs: high-shear mixing and low-shear mixing. High-shear mixers are more efficient than low-shear mixers in terms of generating a formulation with good homogeneity. High-shear mixers are particularly recommended for formulations containing a coating agent since these agents are more easily smeared with high-

shear mixing. However, a drawback of high-shear mixers is their potential to induce the formation of amorphous content, which subsequently lead to stability issues. This effect is greater for larger particles and at higher mixing speeds. Low-shear mixers are suitable, for instance, for binary drug systems, and are typically conducted using a tumbling mixer, such as the Turbula. These mixers are gentle and pose a minimal risk of damaging crystalline particles. However, when dealing with highly cohesive APIs, the applied force might not be sufficient to disperse API agglomerates. [8]

Previous studies have explored the forces exerted among particles in high-shear mixing and their impact on formulation performance, particularly concerning FPF. The applied mixing force can be described according to equation (3): [8]

$$MF = m_{carrier} \times \frac{v^2}{r} \tag{3}$$

Where $m_{carrier}$ is the mass of one carrier particle, v is the peripheral speed, and r is the radius of the mixing bowl. However, the key concept that has been investigated is mixing energy, which can be written as the mixing force multiplied by the distance. See equation (4). [8]

$$ME = \frac{m_{carrier} \times v^3 \times t}{r} \tag{4}$$

Where $m_{carrier}$ is the mass of one carrier particle, ν is the peripheral speed, t is the mixing time, and r is the radius of the mixing bowl. If the equation is to be rewritten with revolutions per minute (rpm), it would instead appear as equation (5): [8]

$$ME = 8\pi^3 \times m_{carrier} \times \left(\frac{rpm}{60}\right)^3 \times r^2 \times t \tag{5}$$

The Turbula mixer has a complex movement pattern, making two 8-shaped cycles for every revolution. This results in a harder prediction of the force exerted on each particle. However, studies have shown that the three main modes in Turbula mixers can be described as centrifugal, rotational, and translational. The centrifugal mode is the main mode giving rise to forces between particles. Meanwhile, the rotational and the translational modes are seen as having less impact on the force field and are often disregarded. The mixing energy for Turbula mixers has been estimated according to equation (6): [23]

$$ME = m_{carrier} \times a \times 2 \times \pi \times r \times t \times 2 \times rpm \tag{6}$$

Where $m_{carrier}$ is the mass of the carrier particle, a is the acceleration, r is the radius of the stirrup, and t is the mixing time in minutes. However, the equation does not include the movement from side to side within the mixing vessel. [23] Furthermore, limited research has been conducted to investigate the impact of different mixing parameters, such as mixing time and speed in the preparation of adhesive mixtures. One study showed that an extended mixing

time did not show a correlation with blend uniformity while in another study it was established that increased mixing time resulted in reduced drug detachment and decreased FPF. [24] Additionally, another study reported an increase in FPF with longer mixing times for batches blended in the Turbula mixer. [23]

3. Materials and methods

The lactose carriers chosen were Lactohale®100 (LH100), Lactohale® 206 (LH206), and Respitose® SV003 due to the difference in size. LH100 has the largest D_{50} value, indicating the largest particle size and SV003 has the smallest D_{50} value, and thus has the smallest particle size. It is important to choose carriers that have significant differences in size to obtain comparable results and to be able to draw a reasonable conclusion. These carriers were also chosen since the % < 10 μm value is low, indicating smaller amounts of fines, see Table 1.

Table 1: Particle size distribution of the lactose carriers.

Carrier	**D_{10} (μm)**	**D_{50} (μm)**	**D_{90} (μm)**	**% < 10 μm**
Lactohale® 100	58	132	214	2
Lactohale® 206	33	83	154	4
Respitose® SV003	31	61	95	3

The API chosen was budesonide and the specifications of all raw materials used are presented in Table 2 below.

Table 2: Specifications of the raw materials used.

Raw material	**Function**	**Supplier**	**Batch number**
Budesonide micronized	API	AstraZeneca	4211059-01
Lactohale® 100	Lactose carrier	DFE Pharma	21D018
Lactohale® 206	Lactose carrier	DFE Pharma	733729
Respitose® SV003	Lactose carrier	DFE Pharma	659173

The batches using the Diosna mixer are presented in Table 3 below. The mixing times and rpms were selected to ensure that batches with the same mixing times exhibited similar mixing energies. This was done to facilitate comparisons between batches based on mixing energy. All batches contained 2,0 % budesonide and 98,0 % lactose, see Appendix A for the formulation composition.

Table 3: Specifications of the batches using the Diosna mixer.

Batch	**Mixer**	**API**	**Carrier**	**Mixing time (min)**	**Rpm**
D-100-2,5	Diosna	Budesonide	LH100	2,5	540
D-100-5	Diosna	Budesonide	LH100	5	540
D-100-9	Diosna	Budesonide	LH100	9	540
D-100-14	Diosna	Budesonide	LH100	14	540

D-206-2,5	Diosna	Budesonide	LH206	2,5	850
D-206-5	Diosna	Budesonide	LH206	5	850
D-206-9	Diosna	Budesonide	LH206	9	850
D-206-14	Diosna	Budesonide	LH206	14	850
D-003-2,5	Diosna	Budesonide	SV003	2,5	1200
D-003-5	Diosna	Budesonide	SV003	5	1200
D-003-9	Diosna	Budesonide	SV003	9	1200
D-003-14	Diosna	Budesonide	SV003	14	1200

Table 4 below shows the batches produced with the Turbula mixer, mixing time, rpm, and the carriers used. All batches contained 2,0 % budesonide and 98,0 % lactose, see Appendix A for formulation composition.

Table 4: Specifications of batches produced using the Turbula mixer.

Batch	**Mixer**	**API**	**Carrier**	**Mixing time (min)**	**Rpm**
T-100-20	Turbula T2C	Budesonide	LH100	10*2	68
T-100-60	Turbula T2C	Budesonide	LH100	30*2	68
T-206-20	Turbula T2C	Budesonide	LH206	10*2	68
T-206-60	Turbula T2C	Budesonide	LH206	30*2	68
T-003-20	Turbula T2C	Budesonide	SV003	10*2	68
T-003-60	Turbula T2C	Budesonide	SV003	30*2	68

3.1 Production of batches

The Diosna batches were produced by first weighing the raw materials. Budesonide was weighed on an analytical scale and lactose was weighed on a regular scale, and the total amount of powder was 250 g. The lactose and budesonide were added to the Diosna mixing vessel (1,2 l) according to the sandwich method, where half of the lactose was added first, then the budesonide, and lastly the rest of the lactose [25]. The powder was initially mixed for 1 minute at 150 rpm and then increased to the actual rpm (540, 850, or 1200). The mixer was stopped at 2,5, 5, 9, and 14 minutes where the temperature of the powder was measured using an IR thermometer. A sample of 40 g was taken out, and powder residues were scraped down from the walls of the mixer by using a scrape card, see Figure 5 for the Diosna mixing vessel set-up. Since samples were taken out by time, the composition of the batches using the same lactose carrier is assumed to be the same.

Figure 5: Picture of the Diosna mixing vessel. Some of the powder attached to the walls of the vessel was obtained for all batches.

The Turbula batches were produced by first weighing budesonide on an analytical scale, and lactose on a regular scale. A mixing vessel was then weighed, and the lactose and budesonide were added to a mixing vessel (glass) by using the sandwich method, previously mentioned. The mixing vessel was then closed and secured with parafilm before it was put in the Turbula T2C mixer, see Figure 6 for the Turbula set-up.

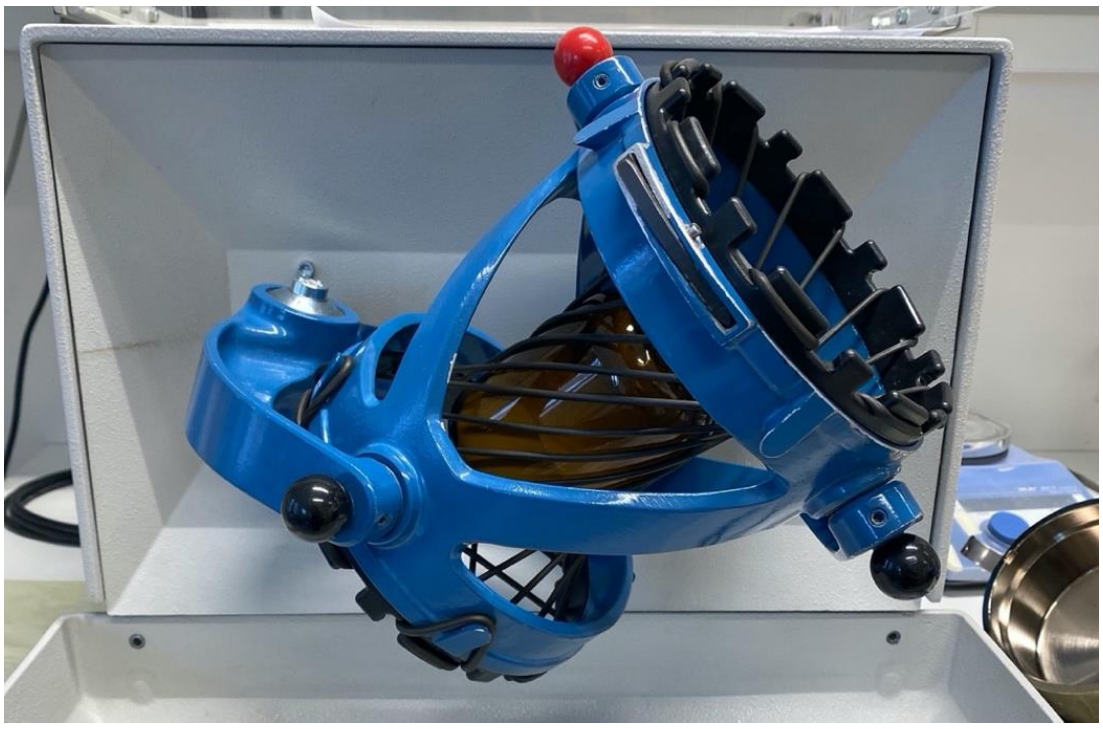

Figure 6: Picture of the Turbula mixer. The glass jar (mixing vessel) with the powder is placed inside the black plastic straps.

The mixing vessel with the powder was mixed for 10 or 30 minutes and then the mixing was stopped. The powder was then sieved by using a 0,71 mm sieve (see Figure 7) and then added back to the mixing vessel. Aggregates of particles were observed during the sieving and were gently pressed through the mesh by using a metal spoon. The powder was then mixed for 10 or 30 minutes more. Lastly, the mixing vessel containing the powder was weighed.

Figure 7: Picture of 0,71 mm sieve with the powder. The sieve was gently shaken, and lumps were gently pressed through the mesh.

3.2 Homogeneity

A calibration curve of budesonide was conducted before the homogeneity measurements of the batches. Pure budesonide was weighed using an analytical scale and diluted with EtOH:H_2O (1:1, by volume), and the concentration ranges were between 0,058 and 0,0036 mg/ml. The absorbance was measured at 246 nm and 350 nm, simultaneously, to minimize background noise, using Varian Cary 50 Bio UV-Visible Spectrophotometer. The absorbance obtained at 350 nm was subtracted from the absorbance obtained at 246 nm. The wavelength of 246 nm has been established in previous studies, which is why it was chosen [26]. The absorbance was plotted against the concentration and the calibration curve is presented in Figure 8.

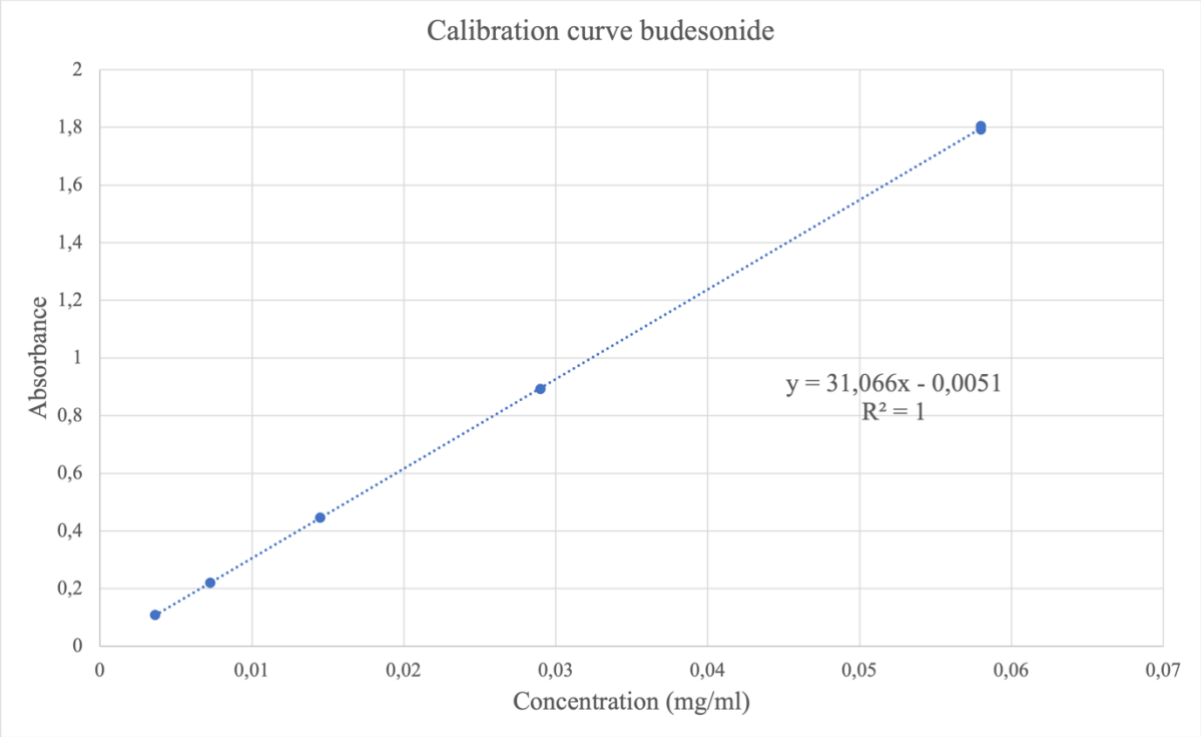

Figure 8: Calibration curve for budesonide.

The homogeneity of the Diosna batches with a mixing time of 2,5 and 5 minutes, as well as Turbula batches with the short mixing time (20 minutes), was performed and suggested homogenous if the relative standard deviation obtained was lower than 5 % [27]. Six samples, varying between 20-40 mg, from different parts of the glass jars, were taken by using metal weighing ships. The samples were added together with the weighing boat in a conical flask and 30 ml of EtOH:H_2O (1:1 by volume) was added and stirred for 15 minutes to ensure complete dissolution of the powder. The solution was visually inspected after 15 minutes. A cuvette (10 mm light path) was filled and then the absorbance was measured. The equation obtained from the calibration curve, equation (7), was used to determine the concentration of budesonide and, subsequently, the amount of budesonide in the samples. The relative standard deviation was calculated to evaluate the homogeneity of the batches [25].

$$y = 31{,}066x - 0{,}0051 \quad (7)$$

3.3 Bulk density

Poured bulk density measurements were performed on each batch, as well as the pure carriers. The batches rested for 4 days after manufacturing before the bulk density measurements to reduce electrostatic effects. Bulk density cylinders were used with a known volume. The outer cylinder was weighed and then zeroed. The inner cylinder was then added to the outer cylinder and the powder was poured into the cylinders using a metal spoon. Furthermore, the inner cylinder was carefully removed so that the powder was flown into the outer cylinder. The excess powder was scraped off using the handle of a metal spoon. The outer cylinder, containing the powder, was then weighed. The volume of the outer cylinder was 20,2 ml. The bulk density was then calculated according to equation (2), see section 2.2.8. See Figure 9 for a schematic picture.

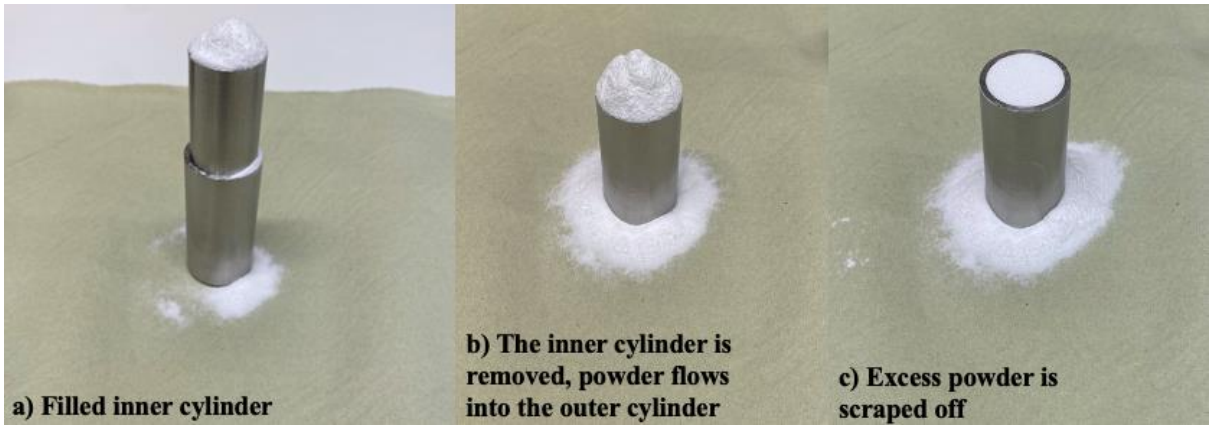

Figure 9: a) The inner cylinder is filled with powder. b) The inner cylinder is removed so that the powder is flown into the outer cylinder. c) The excess powder is gently scraped off with the handle of a metal spoon.

3.4 Next Generation Impactor (NGI)

The capsules were filled by weighing 20-30 mg of the powder, using an analytical scale. The equipment was set up according to the manufacturer and the cups were coated with 0,5 ml Brij/glycerol solution for the small cups, and 1 ml for the larger cups to prevent bounce. The NGI was connected to a TRIG box to control the flow rate and pressure drop. See Figure 10 for the NGI set-up.

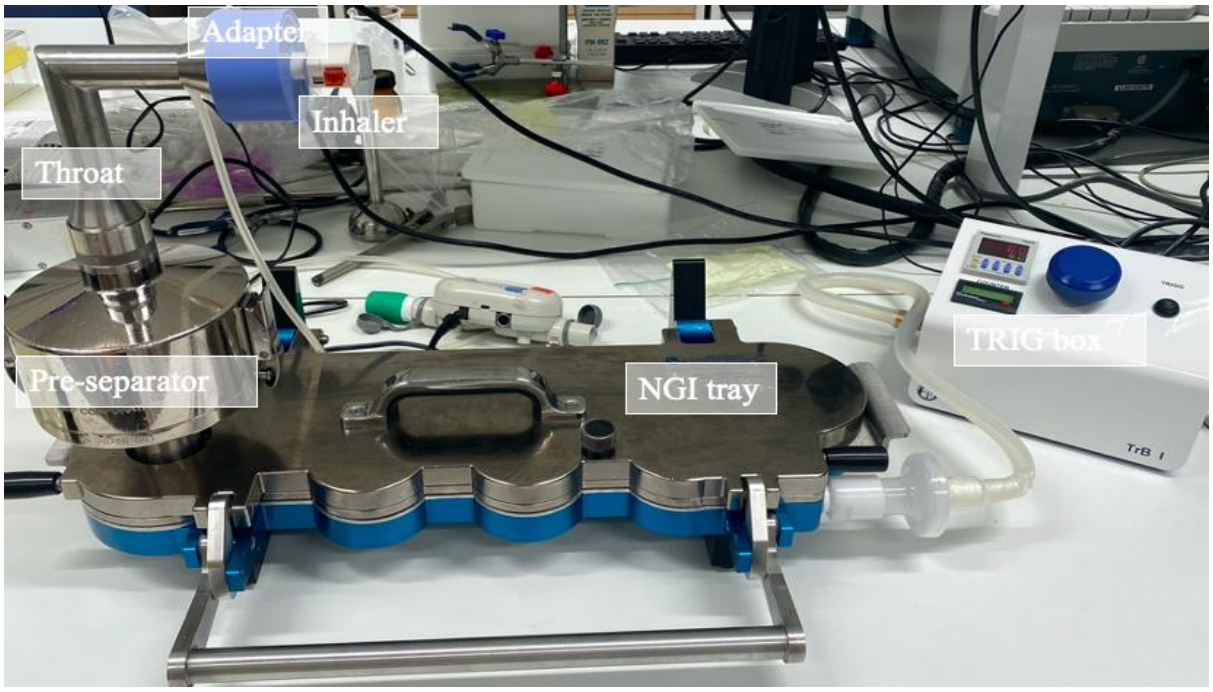

Figure 10: NGI set-up during measurement.

The equipment was calibrated before each measurement by setting the pressure drop to 4kPa by running an empty capsule. After adjusting the pressure drop, the flow rate was tested to ensure it was set correctly (43 l/min). To prevent particles from bouncing, 15 ml of EtOH:H_2O (1:1, by volume) was added to the pre-separator before the experiment started. The inhaler used was a capsule inhaler named RS-01 with a red button.

Firstly, the capsule was added to the inhaler and the capsule was pierced, then, the inhaler was added to the throat, and the experiment was run for 6 seconds. Each batch was tested 3 times, and six capsules were conducted for each replicate (18 capsules were used per batch). See Figure 11 for the stages of the NGI tray.

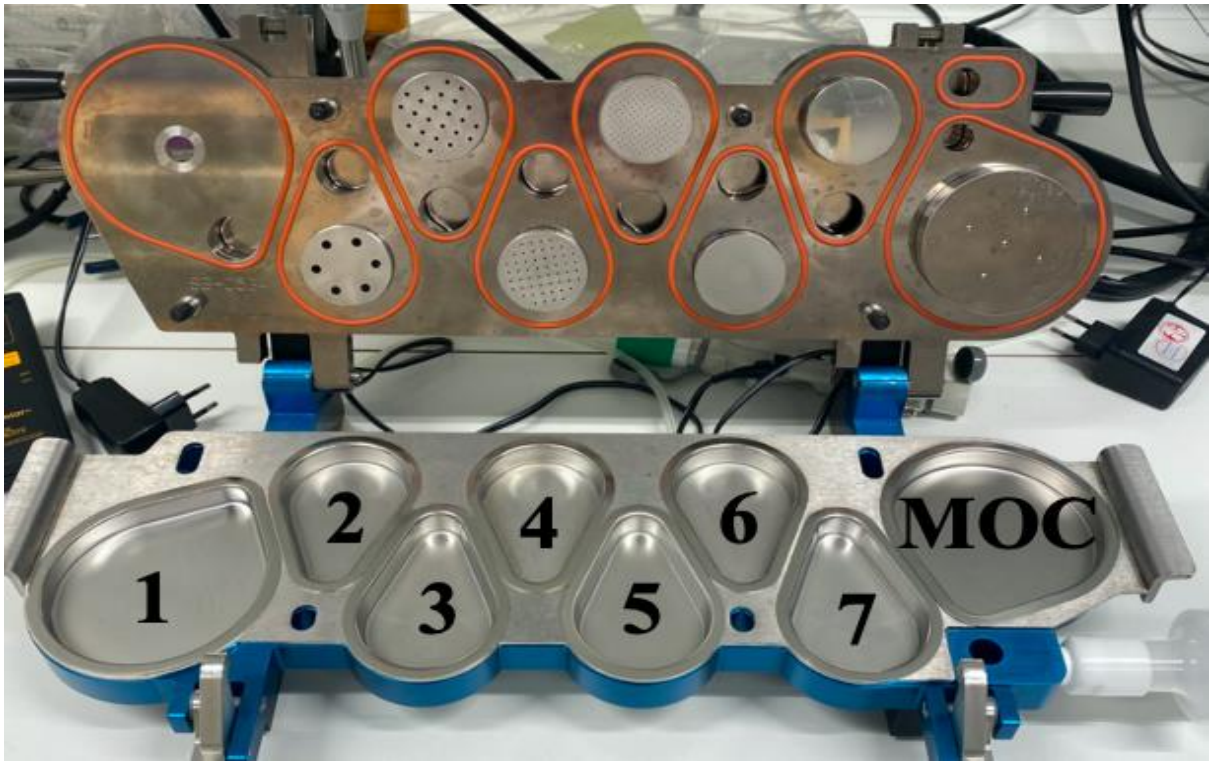

Figure 11: Shows the NGI tray from stage 1 to the MOC.

As mentioned, the pressured drop was set to 4kPa, which resulted in a flow rate of 43 l/min. The cut-off diameters related to this flow rate and pressure drop are presented in Table 5 below.

Table 5: Cut-off diameters of each stage at 43 l/min.

Stage	Cut-off diameters (µm)
1	15,4
2	9,6
3	5,3
4	3,3
5	1,94
6	1,12
7	0,67
MOC	0,43

After 6 capsules, 15 ml of EtOH:H_2O (1:1, by volume) was added to each cup, throat, and the capsules and was set on a mixing table for 15 minutes. Additionally, 15 ml of the EtOH:H_2O solution was added to the pre-separator and shaken thoroughly for 5 minutes. The samples were analyzed by using a Varian Cary 50 Bio UV-Visible Spectrophotometer. The absorbance chosen was 246 and 350 nm, as used in the homogeneity measurements, and the concentration of budesonide was calculated according to the equation generated from the calibration curve (see section 3.2). The concentration of budesonide was further calculated as µg budesonide,

and this value was put in a template given by Emmace Consulting AB that calculated each parameter.

3.5 SprayTec

SprayTec was used to determine the emptying time of the capsules, i.e., how long time it took for the capsules to empty on powder, as well as the particle size distribution of the powders. The batches that were tested were the ones with the shortest and longest mixing times (2,5 and 14 minutes) for each carrier produced in the Diosna mixer. A TRIG box was connected to the instrument and the flow rate was set to 43 l/min. The measurement was run for 6 seconds and at 250 Hz. The set-up of the instrument is presented in Figure 12.

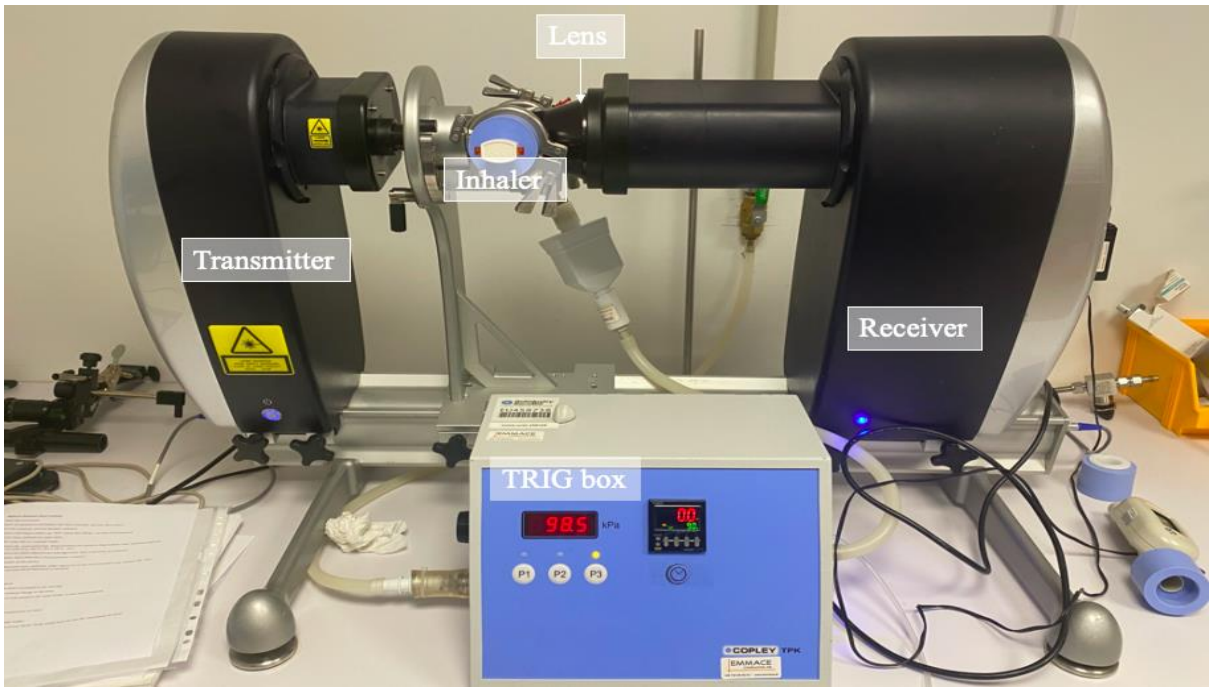

Figure 12: Set-up of the SprayTec instrument with a description of the components.

The emptying time was determined by looking at the "Size and Transmission" diagram (see Figure 13), which showed how the particle size and concentration changed over time. The emptying time was determined by examining the red graph at the top of the diagram, identifying the initial decrease in signal, and measuring the duration until the transmission returned to approximately 98%.

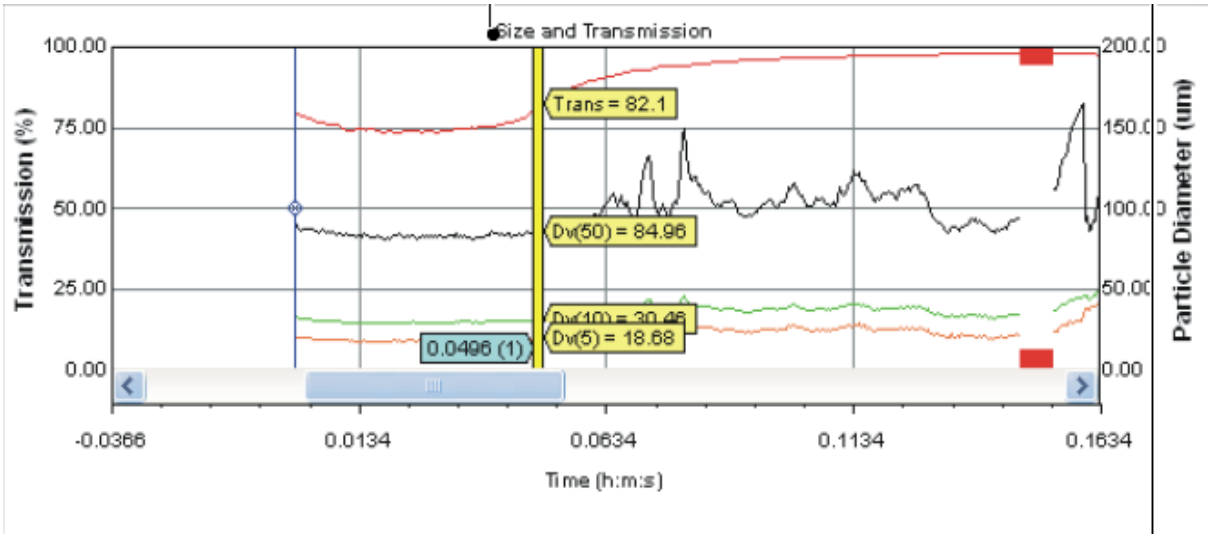

Figure 13: Illustration of the "Size and Transmission" diagram which was used to determine the emptying time of the capsules for each carrier. The emptying time was determined by examining the red graph at the top of the diagram, identifying the initial decrease in signal, and measuring the duration until the transmission returned to approximately 98%.

3.6 Scanning Electron Microscopy (SEM)

Scanning electron microscopy (SEM) was utilized to generate high-resolution images and surface information of the lactose-budesonide particles. SEM testing was conducted on batches produced in the Diosna mixer for each carrier mixed for 2,5 and 14 minutes. Sample preparation involved attaching double-sided adhesive tape to an aluminum stub, onto which a small amount of powder was evenly dispersed. The samples were then ready for sputtering, where the samples were put in a vacuum ($5*10^{-2}$ mbar) to ensure no interference from the air during the process. The surfaces were then coated with approximately 15 nm of Au/Pd to enhance conductivity and prevent charge build-up during SEM analysis. Images were captured using settings of 10 kV and 10 µA. Unfortunately, the image resolution did not meet expectations, with considerable noise present. Nonetheless, for this diploma work, the quality was deemed sufficient.

4. Results and Discussion

In this section, the results from the experiments will be presented. The bulk density and homogeneity measurements will be presented for both the Turbula and Diosna batches, and the aerodynamic particle assessment will be presented for the Turbula and Diosna batches separately.

4.1 Manufacturing

The production yield was calculated for all batches to above 90%. The relative humidity was measured before manufacturing the Diosna batches (at Iconovo) and was approximately 30%, however, the relative humidity was not measured at the lab at The Department of Process and Life Science Engineering. Electrostatic effects of the powders were observed to a very small extent and were not considered a problem during handling.

Three formulations (D-100-14, D-206-14, and D-003-14) were investigated for amorphous content (TAM) and were considered not amorphous. The tests were carried out at Magle Chemoswed.

4.2 Bulk density

The bulk densities of the pure carriers are presented in Figure 14. The lowest bulk density was obtained for SV003, and, surprisingly, LH206 obtained the highest bulk density. During the manufacturing of the batches, it was noted that LH100 showed the best flowability and, thus, it was expected that LH100 would obtain the highest bulk density.

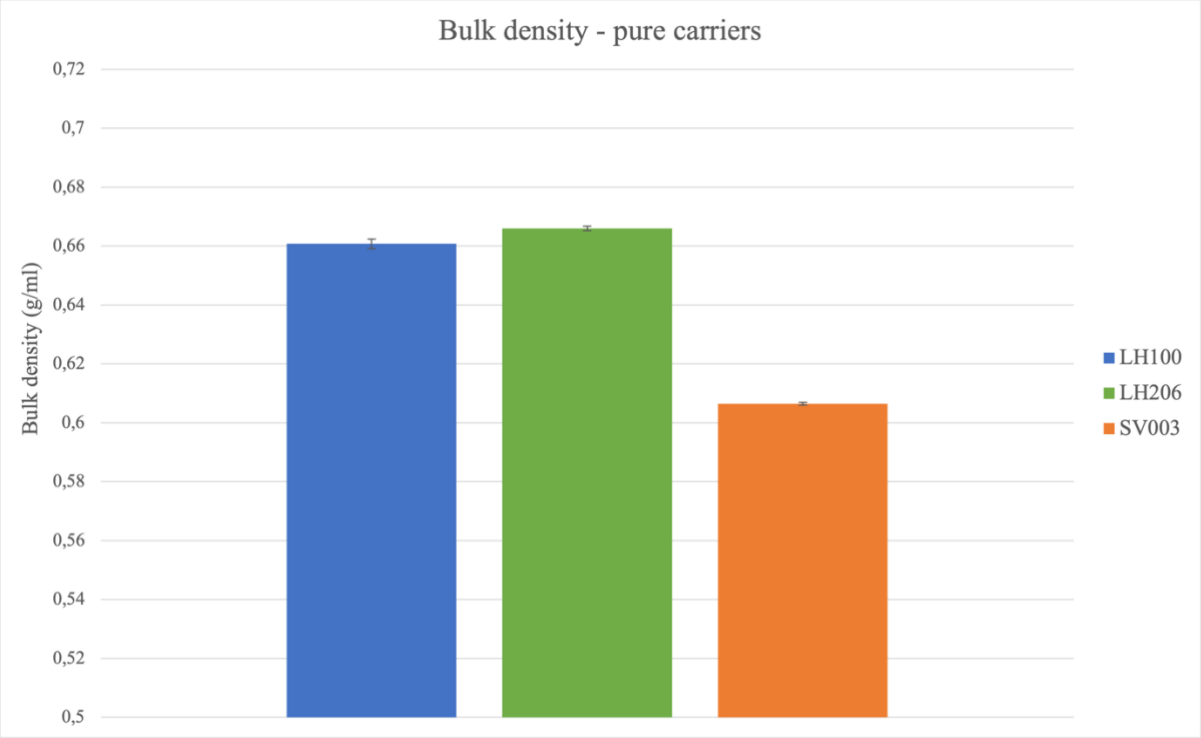

Figure 14: Bulk densities of the pure carriers. The error bars represent the standard deviation.

The bulk densities for the Diosna batches are presented in Figure 15. Batches with LH206 as the carrier yielded the highest bulk densities. This was somewhat surprising since batches with

LH100 as the carrier showed better flowability during handling. However, considering the results observed with the pure carriers, it is reasonable that batches with LH206 achieved the highest bulk density. The bulk density of all batches increased compared to the naked carrier, suggesting that budesonide had been incorporated and adhered to the surfaces of the lactose particles. The bulk densities for the Diosna batches seem to decrease with increased mixing time, which may also result in decreased flowability.

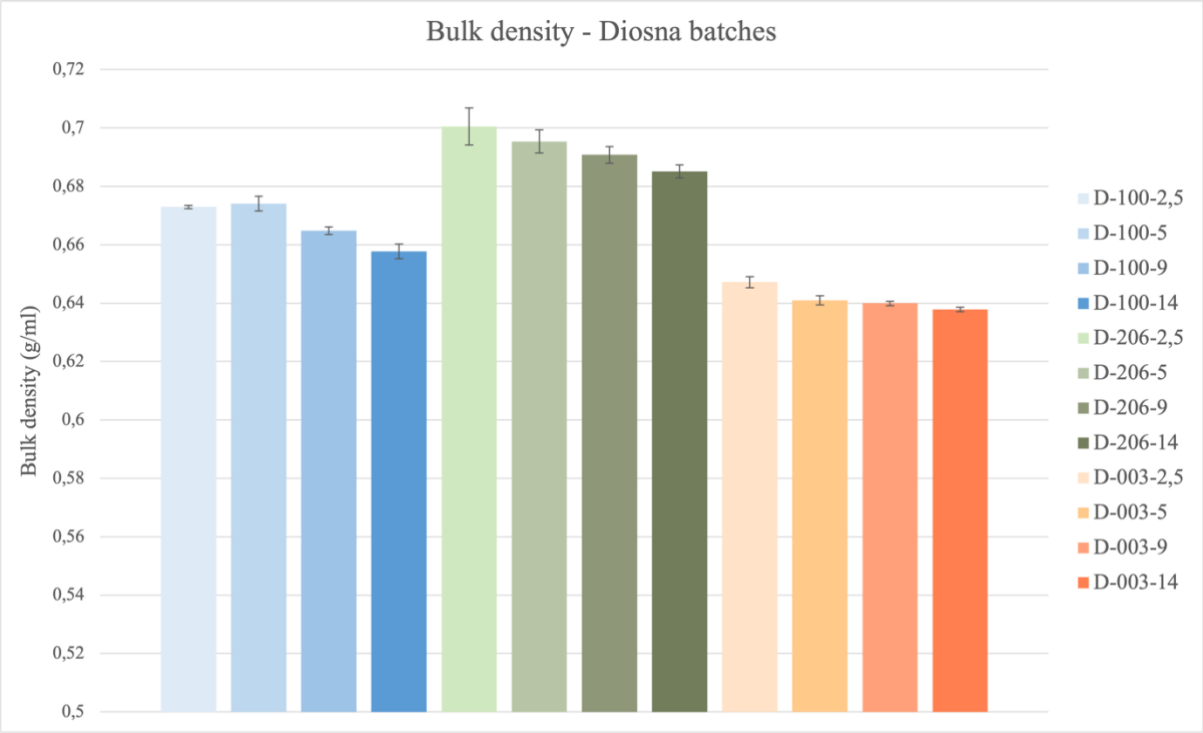

Figure 15: Bulk densities for the Diosna batches. The error bars represent the standard deviation.

The highest bulk density among the Turbula batches was obtained for batch T-206-60, and the lowest bulk density was obtained for batch T-003-20. The batches with LH206 as the carrier obtained the highest bulk density for both the short and long mixing time (see Figure 16). However, it was observed during handling and bulk density measurements that batches with LH100 showed the best flowability. Moreover, based on the bulk density of the pure carriers, it is reasonable that batches containing LH206 exhibited the highest bulk density. Unlike the Diosna batches, the bulk density of the Turbula batches increased with increased mixing time, which may result in increased flowability.

As for the Diosna batches, the bulk density increased compared to the naked carrier, suggesting successful adhesion of budesonide.

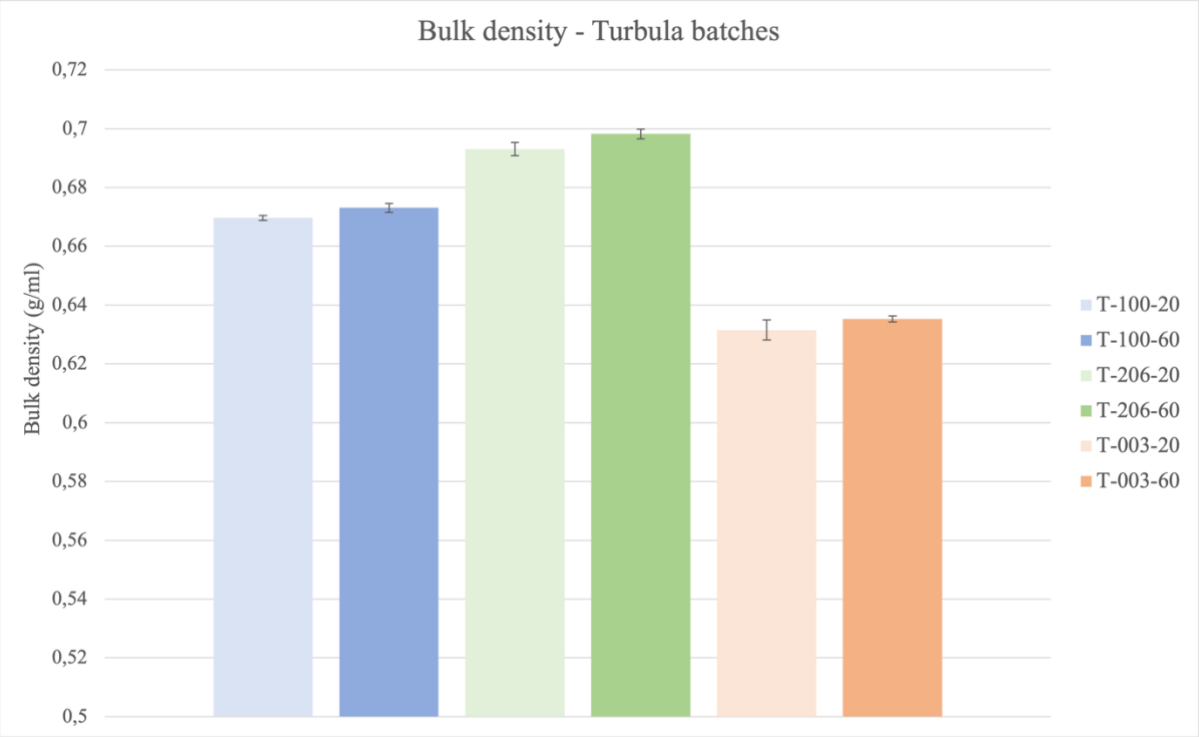

Figure 16: Bulk densities for the Turbula batches. The error bars represent the standard deviation.

Figure 17 shows the bulk density (initial and final) vs. mixing time for the Diosna batches. The initial bulk density was measured 4 days post-manufacturing, and the final bulk density was measured approximately 2 months post-manufacturing. The final bulk density measurements were however only conducted on the shortest (2,5 minutes) and longest (14 minutes) mixing times for the Diosna batches. Comparing the initial and final bulk densities with each other, it is evident that for batches with LH206 and SV003, the final bulk density decreased compared to the initial. For batches with LH100 as the carrier, the initial and final bulk densities were similar. It was expected that the bulk density would increase after 2 months of storage, as the powder might absorb moisture from the air during this period, as well as elimination of electrostatic effects. The greatest difference between the initial and final bulk density was obtained for batches with SV003 as the carrier, however, the differences were small.

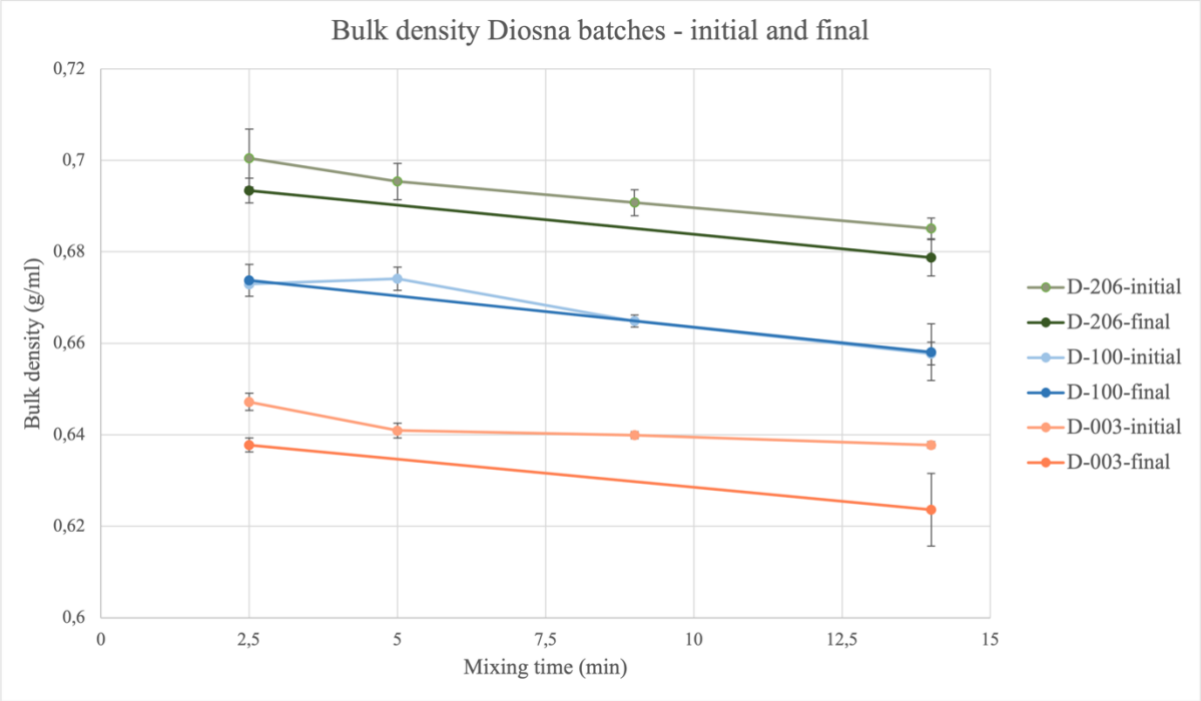

Figure 17: Bulk densities for Diosna batches, initial and final. The initial bulk density was measured four days after manufacturing and the final bulk density was measured approximately two months after manufacturing. The error bars represent the standard deviation.

The initial and final bulk densities for the Turbula batches are presented in Figure 18. As for D-206 and D-003, Turbula batches using LH206 and SV003 as the carriers showed a decrease in final bulk density compared to the initial bulk density. However, for batches with LH100 as the carrier, there was an increase in final bulk density. The differences between initial and final bulk density between different carriers could potentially be explained by differences in relative humidity in the lab. The greatest difference between initial and final bulk density was observed for batches with SV003 as the carrier, a trend also noted for the Diosna batches. An increase in bulk density could be due to factors such as the powder absorbing moisture from the air, or the powder having had time to settle in the glass jar, thereby eliminating any electrostatic effects.

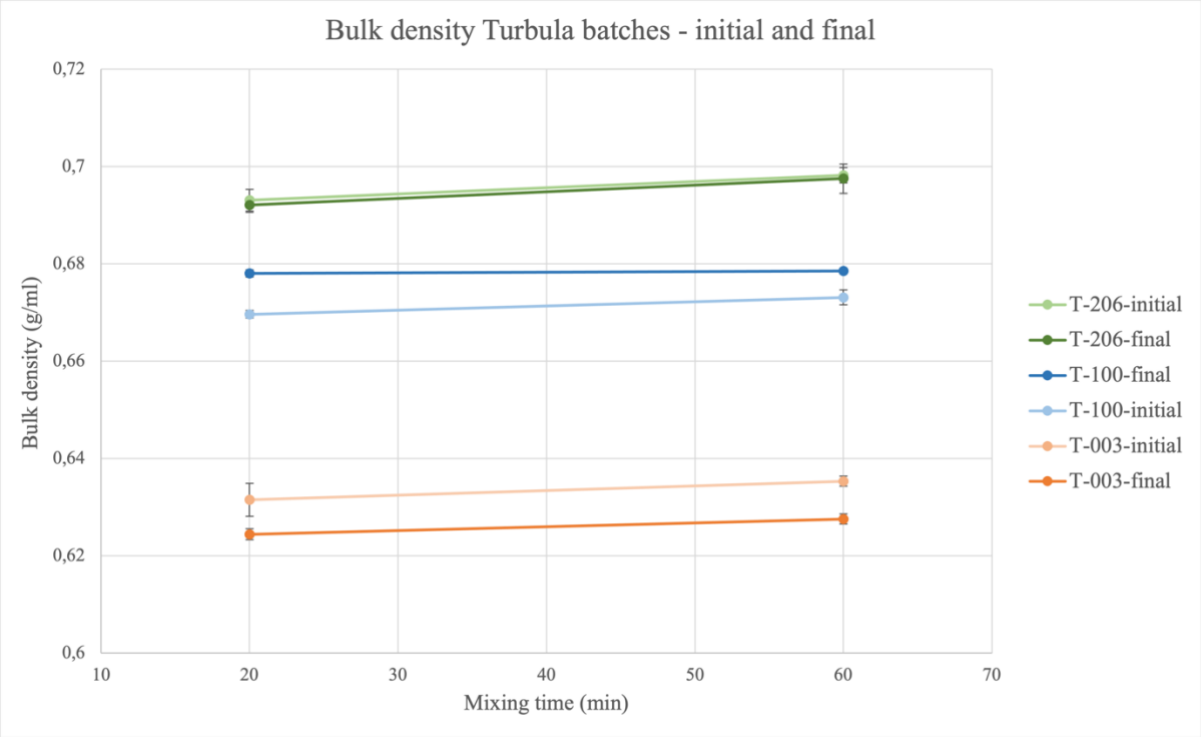

Figure 18: Bulk densities for Turbula batches, initial and final. The initial bulk density was measured four days after manufacturing and the final bulk density was measured approximately two months after manufacturing. The error bars represent the standard deviation.

4.3 Budesonide concentration and homogeneity

The concentration of budesonide in the Diosna batches is presented in Figure 19. All batches displayed a concentration of budesonide slightly above 2%, indicating a greater loss of lactose than budesonide during manufacturing. The homogeneity measurements were conducted on the batches with mixing times of 2,5 and 5 minutes. There were no trends observed regarding mixing time or type of lactose particle.

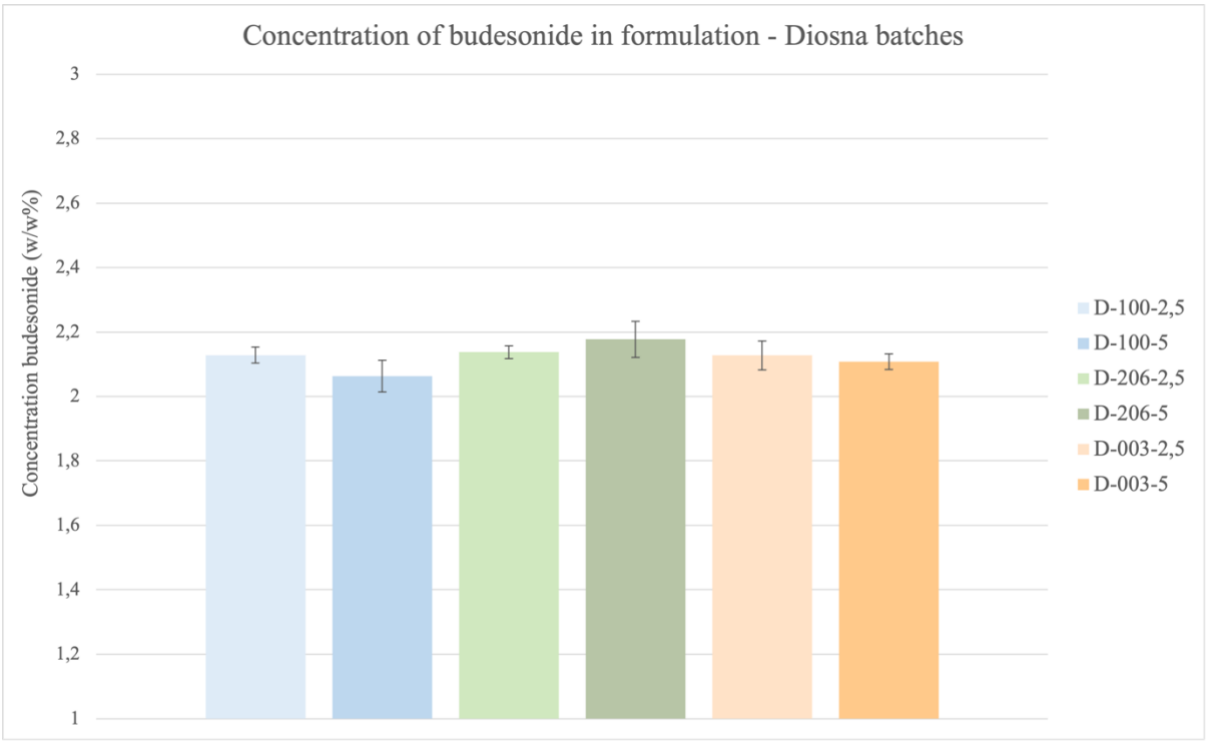

Figure 19: Concentration of budesonide in the Diosna batches mixed for 2,5 and 5 minutes. The error bars represent the standard deviation.

The concentration of budesonide in the Turbula batches with the lowest mixing time (20 minutes) is presented in Figure 20. All batches displayed a concentration of budesonide slightly above 2%, again, indicating a greater loss of lactose than budesonide during manufacturing. The concentration of budesonide increased with decreased lactose particle size.

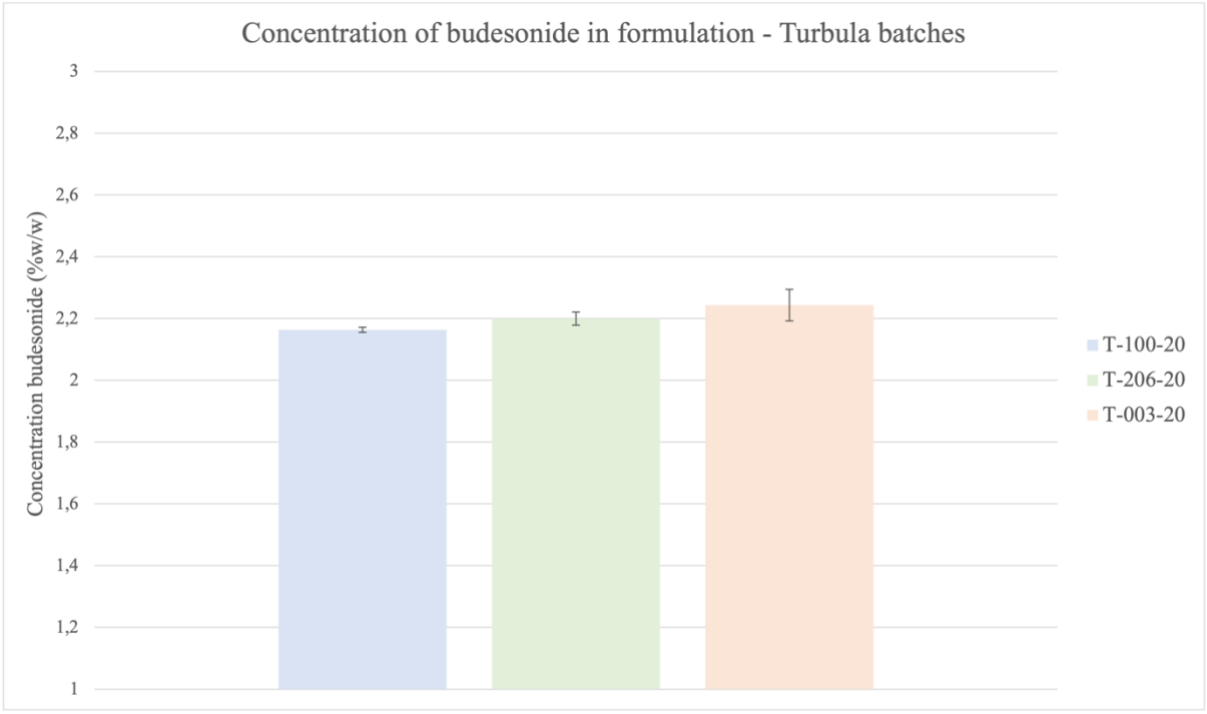

Figure 20: Concentration of budesonide in the Turbula batches mixed for 20 minutes. The error bars represent the standard deviation.

The relative standard deviation of the budesonide concentration was used to determine whether the batches were homogenous or not. From Figure 21, it is evident that the relative standard deviation was lowest for Diosna batches with the shorter mixing time, except for batches with SV003 where the opposite was observed. For the Turbula batches, the relative standard deviation increased with smaller lactose carrier particles. Furthermore, the conclusion drawn from the homogeneity measurements for the Turbula batches was that the larger the carrier particle, the more homogenous the powder. This could potentially be explained by that the larger lactose particles better destroy budesonide aggregates in the Turbula mixer.

For all batches, the relative standard deviation was lower than 5%, indicating homogenous powders. Batches with longer mixing times were thus assumed to be homogenous.

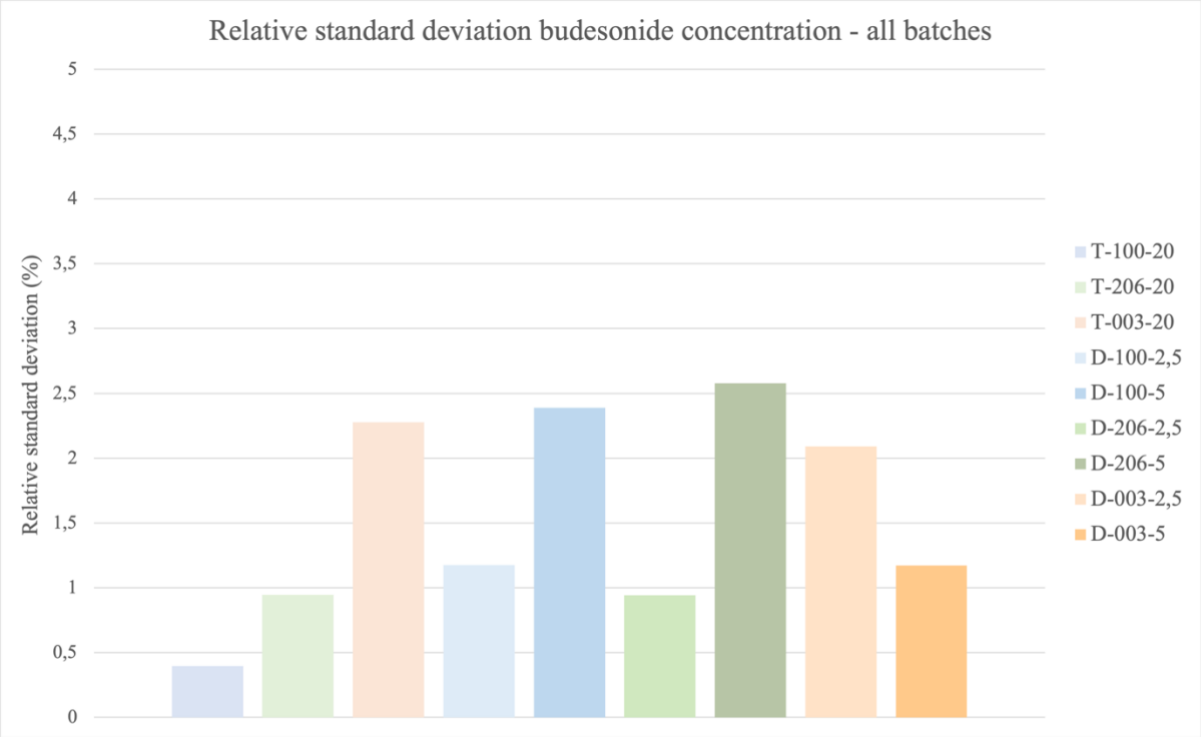

Figure 21: The relative standard deviation (%) of budesonide concentration measurements.

4.4 Aerodynamic particle assessment – Diosna batches

In this section, the NGI results of the Diosna batches are presented. The data from NGI measurements is provided in Appendix B.

4.4.1 Delivered dose and impact on pre-separator and throat

The delivered dose (i.e., the sum of budesonide collected in the throat, pre-separator, and all stages of the NGI) is presented in Figure 22. For batch D-100-5, the amount of powder per replicate (i.e., 6 capsules) was approximately 10 mg lower compared to D-100-2,5, which is an explanation for why the delivered dose decreased between batches D-100-2,5, and D-100-5. For batch D-206-2,5, the amount of powder was also approximately 10 mg lower compared to the other batches in the D-206-series. This difference could potentially account for the lower delivered dose. For the remaining batches, there appears to be a slight increase in the delivered dose with longer mixing times, or the dose remains relatively stable. The highest delivered dose

was observed for batches with SV003 as the carrier, indicating that more of the powder in the capsules entered the NGI.

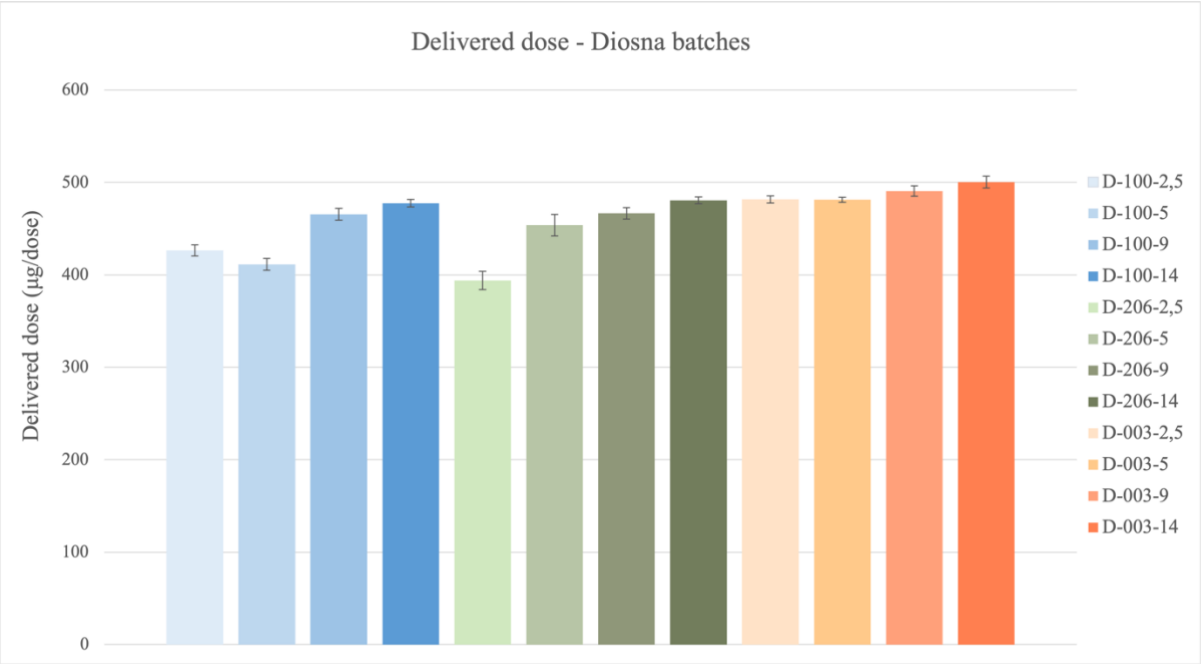

Figure 22: Delivered doses for the Diosna batches, calculated as the sum of budesonide (in µg/dose) on each stage (including pre-separator and throat). The error bars represent the standard deviation.

To determine the impact on the upper parts of the NGI, the fraction of budesonide deposited in the pre-separator and throat was calculated, see Figure 23. The overall trend was that the amount of budesonide that impacted the pre-separator and throat increased with increased mixing time. This could be explained by that when the powder is mixed for longer times, the adhesive forces between budesonide and the carrier particles increase, preventing budesonide from detaching. Batches with the same mixing time seem to show a similar impact on the pre-separator and throat when LH100 and LH206 are used as carriers. However, batches with SV003 as the carrier exhibited a slightly lesser impact on the pre-separator and throat compared to those using other carrier particles.

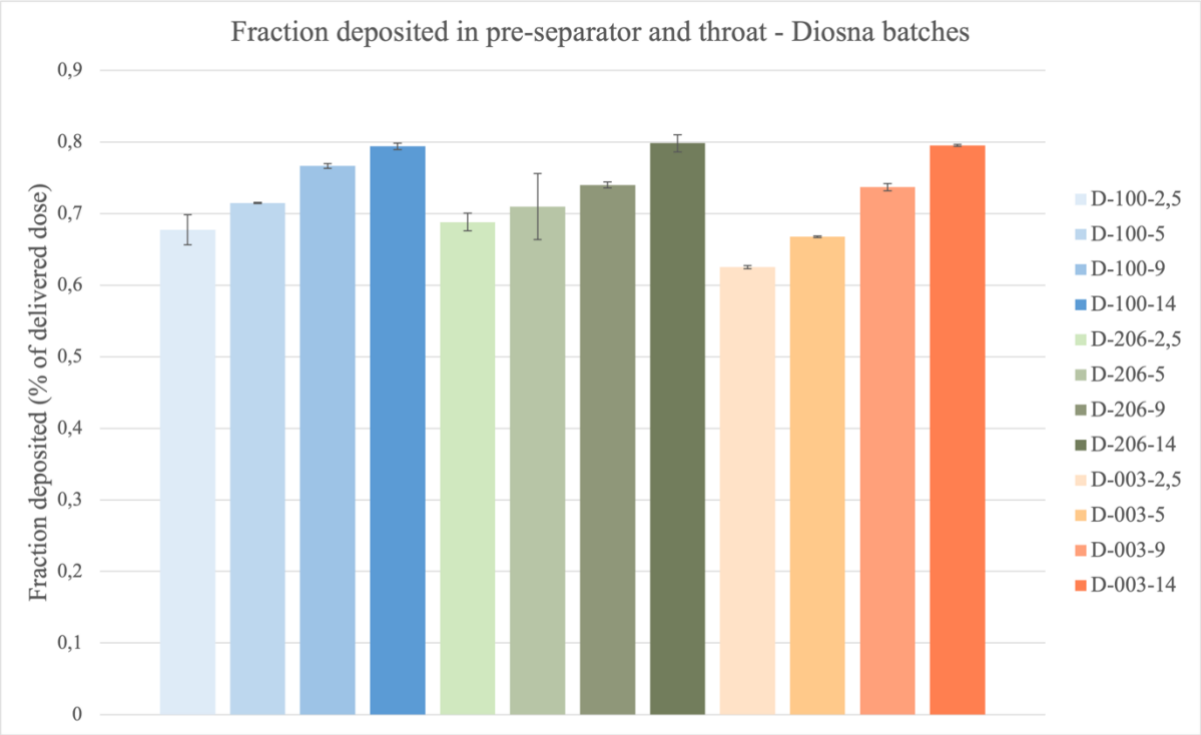

Figure 23: Fraction deposited in the pre-separator and throat for the Diosna batches, calculated as % of delivered dose. The error bars represent the standard deviation.

4.4.2 Fine particle dose

The fine particle dose of the Diosna batches is presented in Figure 24. The highest FPD was obtained for the batches containing SV003 as the carrier and the FPD decreased with increased mixing time. Since the fraction deposited in the pre-separator and throat increased with prolonged mixing, it was reasonable that FPD decreased with increased mixing time. Furthermore, it was unexpected that the FPD increased between the batches D-206-2,5 and D-206-5, as this was not seen in any of the other batches. A probable reason was that the amount of powder used per replicate in D-206-2,5 was approximately 10 mg lower compared to the other batches in the D-206 series.

Figure 24: FPD for the Diosna batches (defined as µg/dose < 5 µm). The error bars represent the standard deviation.

4.4.3 Fine particle fraction

The fine particle fraction of the Diosna batches is presented in Figure 25. The FPF of the Diosna batches decreased with increased mixing time. The overall highest FPF was obtained for the batches with SV003 as the carrier and the lowest FPF was obtained for the batches with LH100 as the carrier. The high FPF values for batches with SV003 could potentially be explained by that budesonide is more evenly spread out on SV003 and that the adhesive forces between the lactose and budesonide are optimal.

Figure 25: FPF for the Diosna batches (defined as % < 5 µm of delivered dose). The error bars represent the standard deviation.

4.4.4 Mass median aerodynamic diameter (MMAD)

The mass median aerodynamic diameter (MMAD) for the Diosna batches is presented in Figure 26. The MMAD tends to increase with longer mixing times, which aligns with the decrease in FPF associated with prolonged mixing. The lowest MMAD obtained was for batches with SV003 as the carrier, which is expected since these batches obtained the highest FPF. However, for batches mixed for 2,5 minutes, the lowest MMAD was obtained for D-100-2,5 which does not align with the results from the FPF.

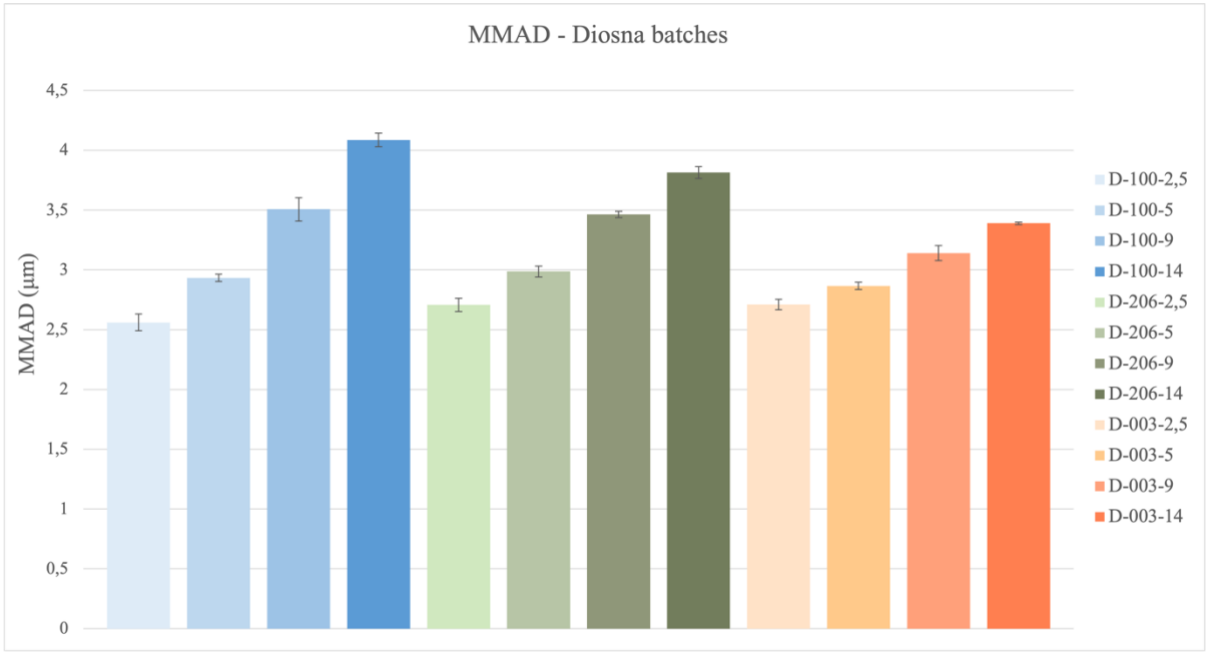

Figure 26: MMAD (in µm) for the Diosna batches. The error bars represent the standard deviation.

4.4.5 Capsule retention

The capsule retention (i.e., the percentage of the total dose that is left in the capsule upon inhalation) of the Diosna batches is presented in Figure 27. For batches with LH100 and LH206, there was a decrease in capsule retention with increased mixing time. The biggest difference for these batches was between 2,5 and 5 minutes. For batches with SV003 as the carrier, the capsule retention increased between 2,5 and 5 minutes, followed by a decrease with prolonged mixing.

For batches with SV003, the total dose was significantly higher compared to batches with LH100 and LH206. Furthermore, the total dose for D-206-2,5 was lower compared to the other batches in the D-206-series. This could account for the lower capsule retention for SV003 as well as the high capsule retention for D-206-2,5. See Appendix B for the exact total doses.

The experimental method for capsule retention was not optimal. The capsules were dissolved in EtOH:H_2O solution, which introduced plastic into the measuring cuvettes. Consequently, this result may not be trusted completely. Furthermore, this could account for the high standard deviations observed.

Figure 27: Capsule retention for the Diosna batches (defined as % of total dose left in capsule upon inhalation). The error bars represent the standard deviation.

4.4.6 SprayTec: Emptying time and particle size

The emptying time of the capsules is presented in Figure 28. The emptying time for the shorter mixing time was roughly 1 second, and slightly shorter for the longer mixing time. Unfortunately, the standard deviation of the measurements was high, however, there seems to be a decrease in capsule emptying time with increased mixing time. This was unexpected since the bulk density decreased with increased mixing time, thus, resulting in decreased flowability.

However, this could stem from for example electrostatic charges between the powder and plastic capsule upon inhalation.

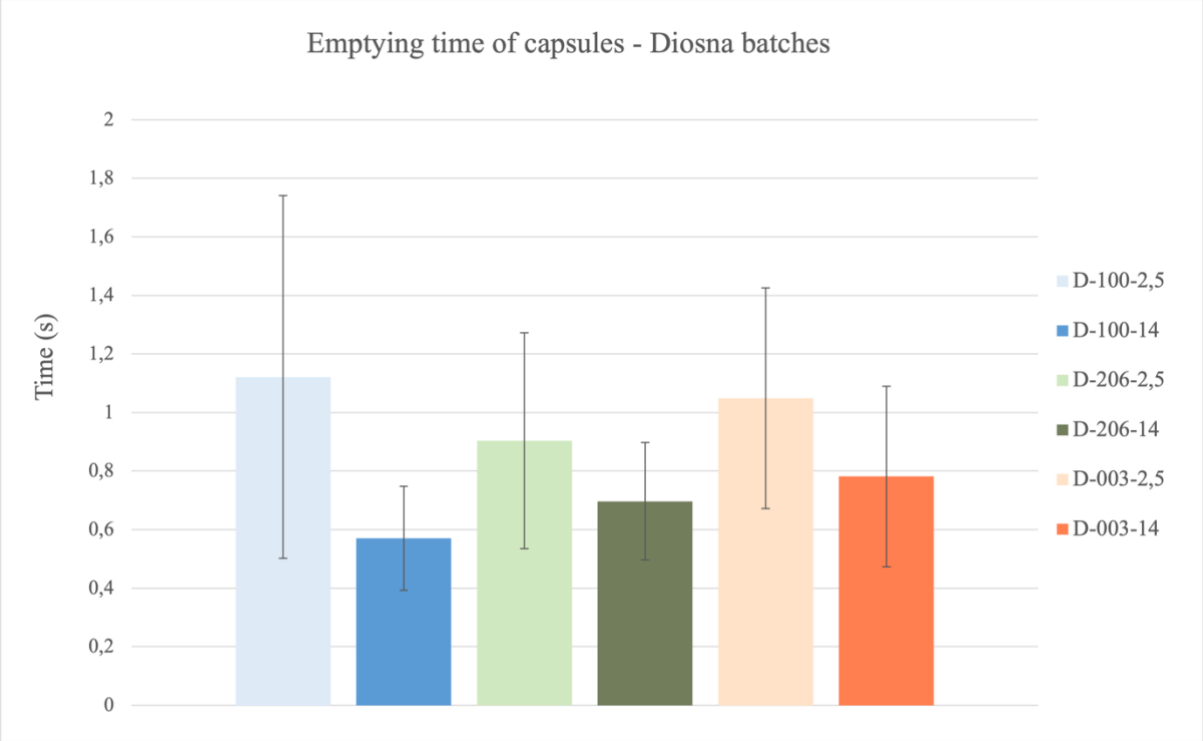

Figure 28: Emptying time of capsules for Diosna batches. The error bars represent the standard deviation.

The results from the particle size assessment from SprayTec are presented in Figure 29. The batches that were tested were the Diosna batches mixed for 2,5 and 14 minutes. According to Figure 29, it is evident that batches with LH100 as the carrier obtained the largest Dv(50) value and that batches with SV003 as the carrier obtained the lowest Dv(50) value. For batches with LH100 and SV003 as carriers, the Dv(50) value seems to be relatively constant. For batches with LH206, there was an increase in Dv(50) with an increased mixing time. Additionally, it would be expected that the Dv(50) value would increase more, especially for batches with LH100 and SV003, considering the decrease in FPF with prolonged mixing times.

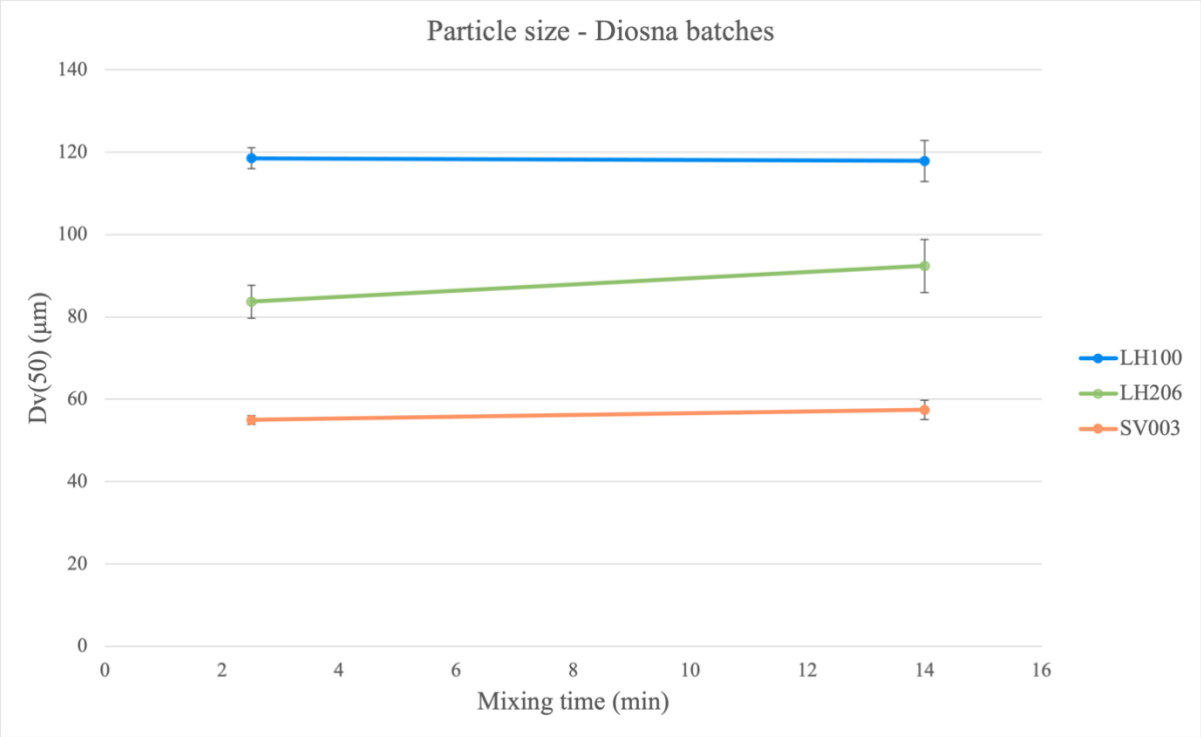

Figure 29: Dv(50) for Diosna batches mixed for 2,5 and 14 minutes. The error bars represent the standard deviation.

4.5 Aerodynamic particle assessment - Turbula batches

In this section, the NGI results of the Turbula batches will be presented. The data obtained from NGI measurements is provided in Appendix C.

4.5.1 Delivered dose and impact on pre-separator and throat

The delivered dose of the Turbula batches is presented in Figure 30. The delivered dose was stable between the batches, considering the standard deviation. The mass per replicate (i.e., per 6 capsules) was approximately consistent, which could contribute to the stable delivered dose.

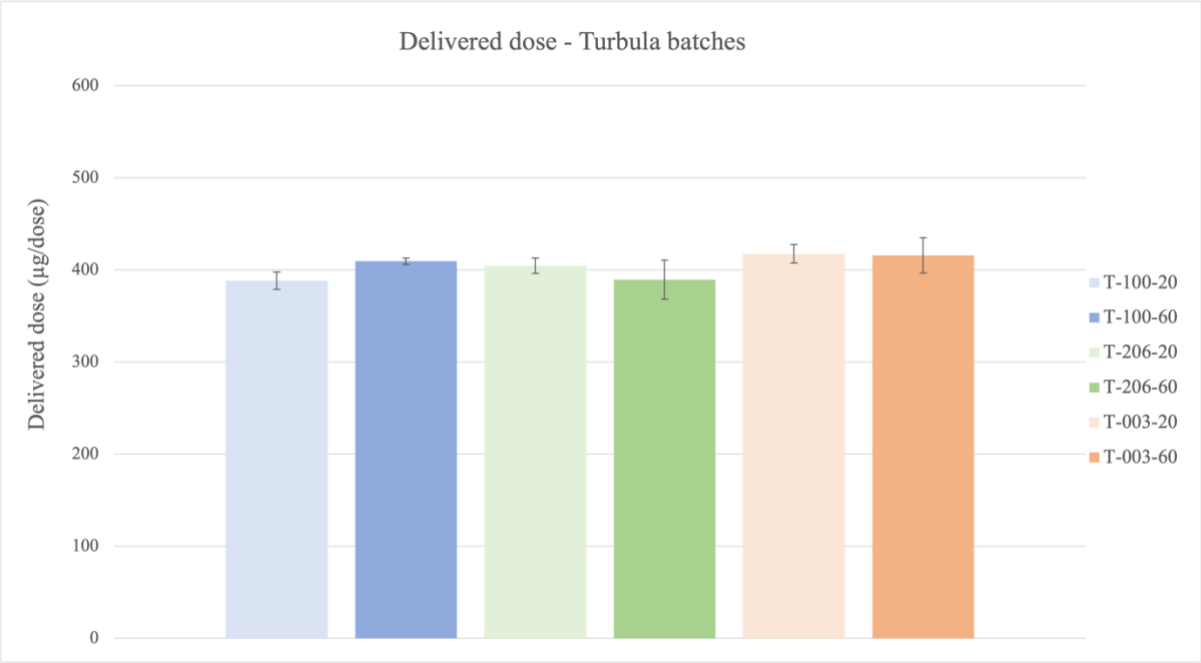

Figure 30: Delivered dose of the Turbula batches, calculated as the sum of budesonide (in µg) on each stage (including pre-separator and throat). The error bars represent the standard deviation.

The amount of budesonide impacting the pre-separator and throat is illustrated in Figure 31. Unlike the Diosna batches, there was a decrease in the amount of budesonide impacting the pre-separator and throat with increased mixing time for the Turbula batches with LH100 and LH206 as carriers. For batches with SV003 as the carrier, the amount of budesonide impacting the pre-separator and throat remained relatively constant. This trend could be explained by that the Turbula mixer is gentler and has a completely different movement pattern, compared to the Diosna mixer. Additionally, longer mixing times in the Turbula mixer may facilitate better distribution of budesonide into the lactose particles, resulting in fewer large budesonide aggregates affecting the pre-separator and throat.

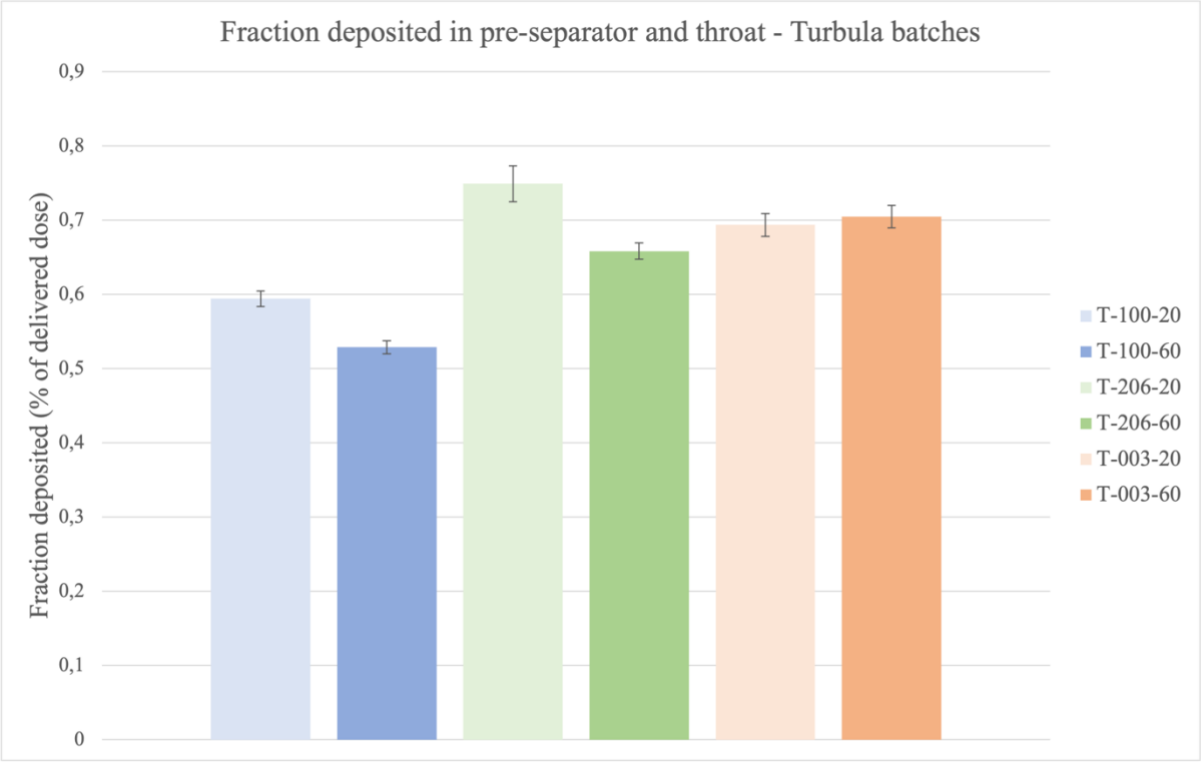

Figure 31: Fraction deposited in the pre-separator and throat for the Turbula batches, calculated as % of delivered dose. The error bars represent the standard deviation.

4.5.2 Fine particle dose

The fine particle dose for the Turbula batches is presented in Figure 32. The FPD increased with increased mixing time for batches with LH100 and LH206, which is the opposite trend compared to the Diosna batches. For batches with SV003 as the carrier, the FPD instead decreased with increased mixing time. The highest FPD was observed for batches with LH100 as the carrier and the lowest FPD was observed for T-206-20, unlike the Diosna batches where the highest FPD was obtained for batches with SV003 as the carrier. It is reasonable to expect that batches with LH100 as the carrier would reach higher FPD, as these batches also showed the lowest impact on the pre-separator and throat. Moreover, T-206-20 displayed the highest impact on the pre-separator and throat, which supports why the FPD of this batch is the lowest.

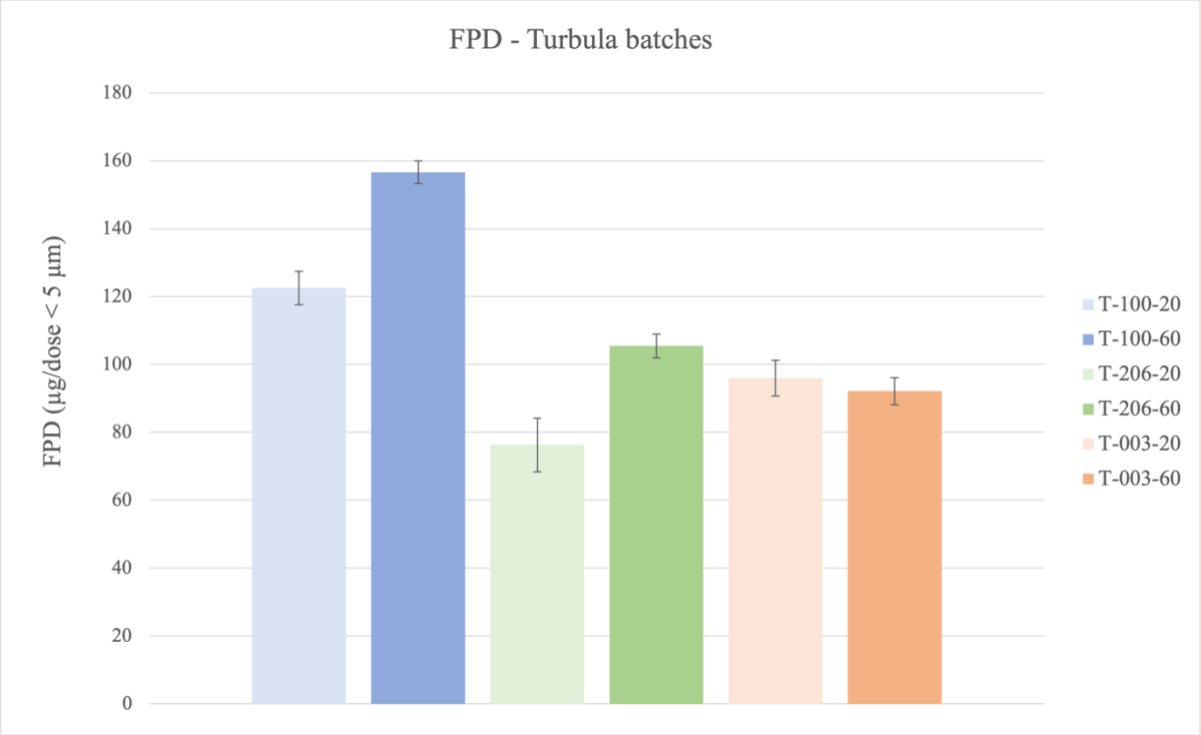

Figure 32: FPD for the Turbula batches (defined as µg/dose < 5 µm). The error bars represent the standard deviation.

4.5.3 Fine particle fraction

The fine particle fraction of the Turbula batches is presented in Figure 33. The Turbula batches with LH100 as the carrier yielded the highest FPF, while those with SV003 as the carrier reached the lowest FPF. This trend is consistent with the FPD trend observed, as a higher FPD implies a higher FPF. There was also a trend of increased FPF with longer mixing times for batches with LH100 and LH206. However, for batches with SV003, there appears to be a slight decrease in FPF with longer mixing times.

It is worth noting that the highest FPF among all batches (both Turbula and Diosna) was achieved by batch T-100-60, at approximately 38%.

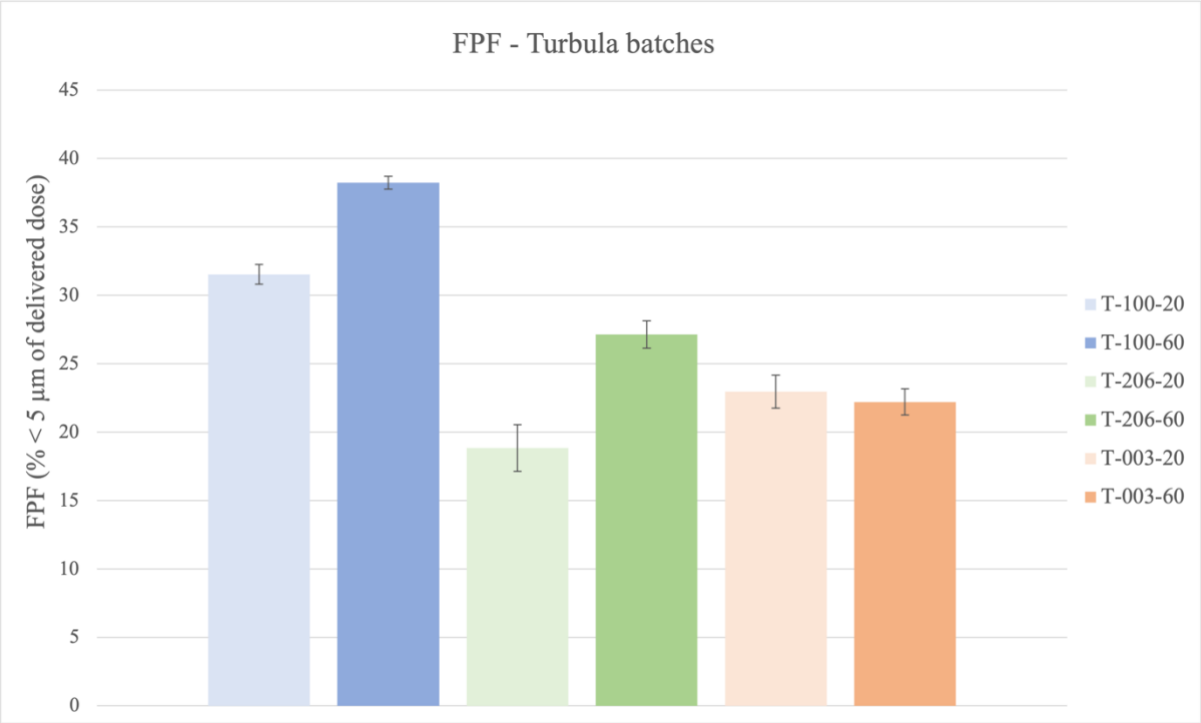

Figure 33: FPF for the Turbula batches (defined as % < 5 µm of delivered dose). The error bars represent the standard deviation.

4.5.4 Mass median aerodynamic diameter (MMAD)

The MMAD of the Turbula batches is presented in Figure 34. There was a trend of decreased MMAD with increased mixing time for batches with LH100 and LH206, which aligns with the increase in FPF observed with longer mixing times. For batches with SV003, there was an increase in MMAD with increased mixing time. However, considering the decrease in FPF for these batches with longer mixing times, this trend is reasonable. The opposite trend was observed for the Diosna batches.

Comparing the MMAD results between the Diosna and Turbula batches, it would be expected that batch T-100-60 would yield the lowest MMAD, as this batch obtained the highest FPF among all batches. Instead, the lowest MMAD was observed for batch D-100-2,5.

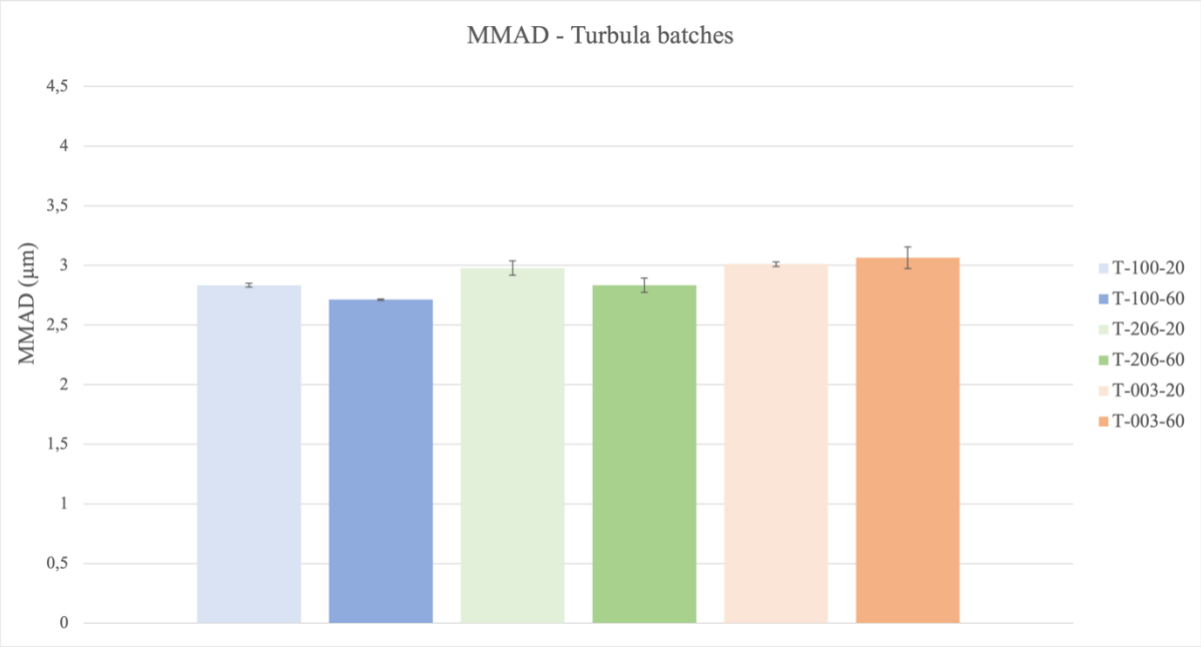

Figure 34: MMAD (in µm) for the Turbula batches. The error bars represent the standard deviation.

4.5.5 Capsule retention

The capsule retention of the Turbula batches (i.e., how many percentages of the total dose are left in the capsules upon inhalation) is presented in Figure 35. As for the Diosna batches, there appears to be a trend of decreased capsule retention with increased mixing time for batches with LH100 and LH206. Furthermore, the capsule retention for SV003 was relatively stable which could be explained by that the total dose for these batches was stable. However, as mentioned in section 4.4.5, the experimental method was not optimal which is why the standard deviations are high.

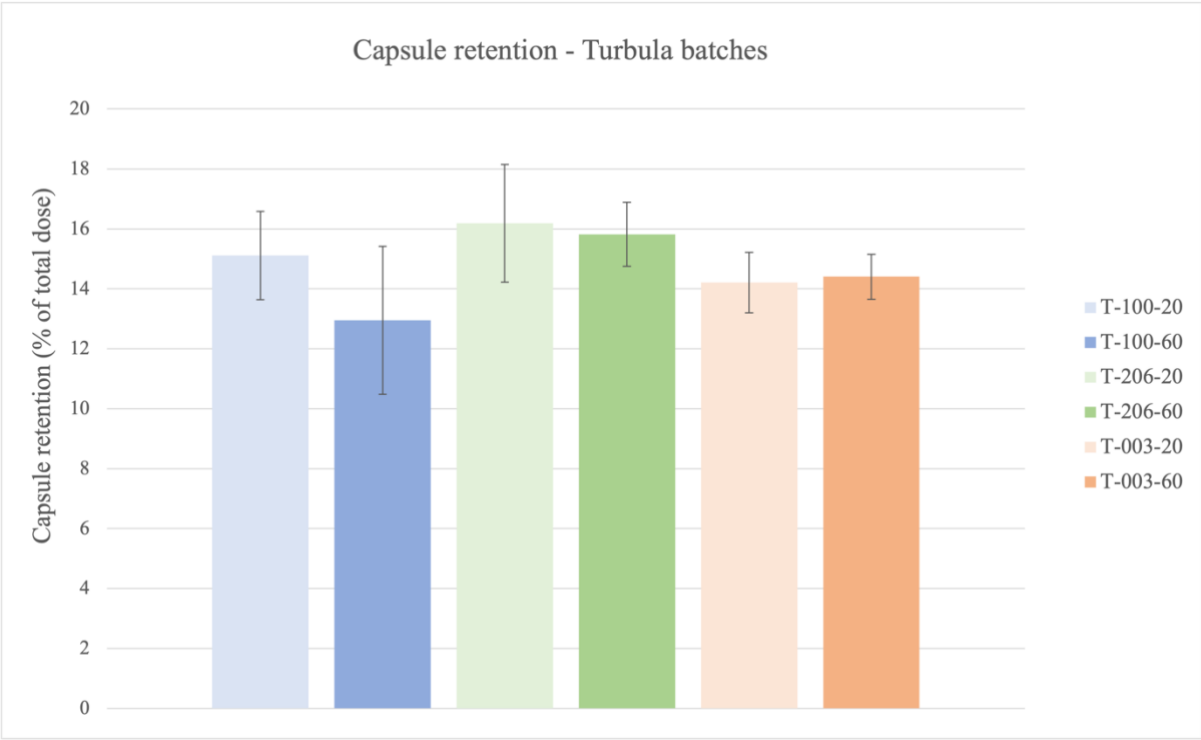

Figure 35: Capsule retention of Turbula batches (defined as % of total dose). The error bars represent the standard deviation.

4.6 Surface morphology (SEM images)

Scanning Electron Microscopy (SEM) was used to reveal the surface morphology of some of the batches. The batches chosen were the Diosna batches with a mixing time of 2,5 and 14 minutes (i.e., the longest and the shortest mixing times). Unfortunately, there were issues with the resolution of the images during the measurement, resulting in differences in quality between the images.

For D-100-2,5 (Figure 36), there were visible spots of what could be budesonide when looking at the images with higher magnification (X500 and X3000). The shape of the lactose particles (for all batches) looks like a tomahawk shape, like a typical adhesive mixture.

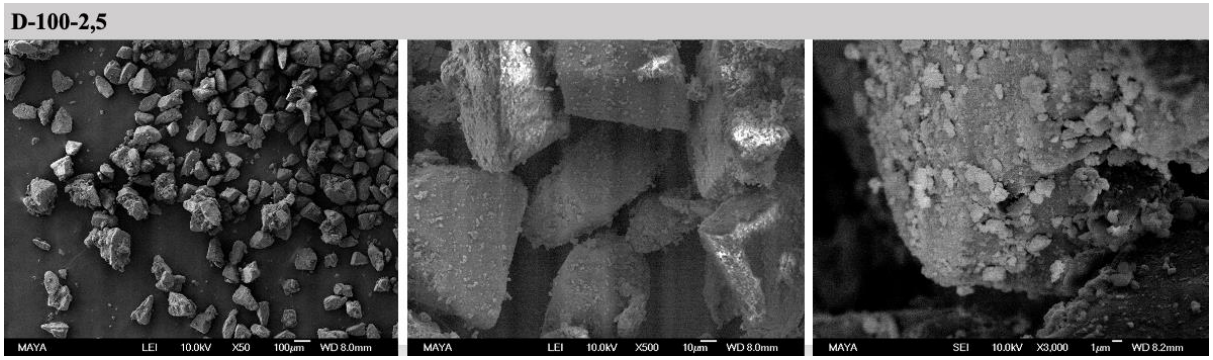

Figure 36: SEM images of batch D-100-2,5. The images were taken at an acceleration voltage of 10,0 kV, a working distance of 8, 8, and 8,2 mm, and a magnification of X50, X500, and X3000 respectively. The detector used was the lower secondary electron detector (LEI) and the in-lens secondary electron detector (SEI).

For batch D-206-2,5 (Figure 37), there seem to be larger agglomerates on the lactose particles (X3000) compared to batch D-100-2,5, potentially budesonide or lactose fines.

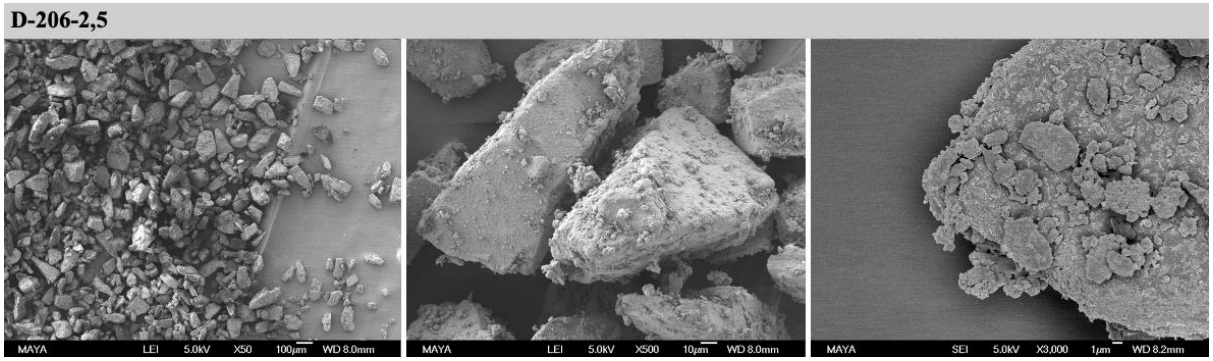

Figure 37: SEM images of batch D-206-2,5. The images were taken at an acceleration voltage of 5,0 kV, a working distance of 8, 8, and 8,2 mm, and a magnification of X50, X500, and X3000 respectively. The detector used was the lower secondary electron detector (LEI) and the in-lens secondary electron detector (SEI).

For batch D-003-2,5 (Figure 38), there were larger agglomerates on the lactose particles. It is, however, hard to know if it is larger agglomerates of budesonide or if it is lactose fines.

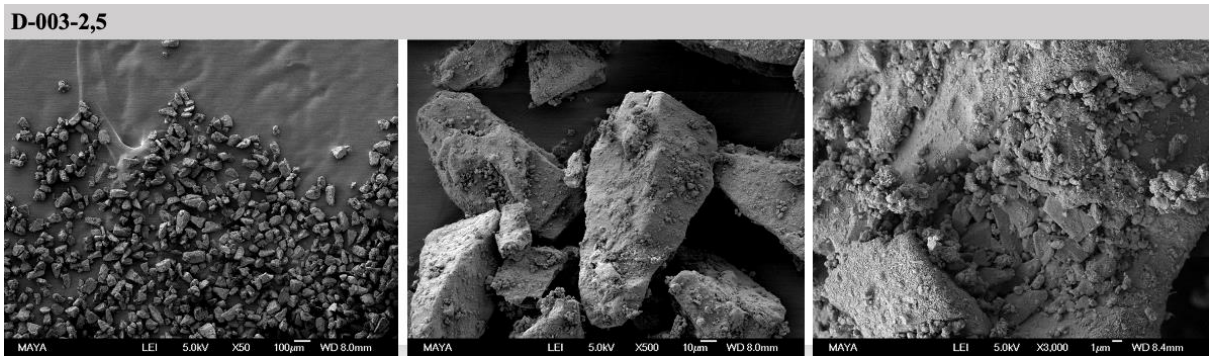

Figure 38: SEM images of batch D-003-2,5. The images were taken at an acceleration voltage of 5,0 kV, a working distance of 8, 8, and 8,4 mm, and a magnification of X50, X500, and X3000 respectively. The detector used was the lower secondary electron detector (LEI).

When examining batches subjected to longer mixing times (see Figures 39-41), it is evident that smaller, needle-like particles are consistently visible on the surfaces of the lactose particles, compared to shorter mixing times. This result can be explained by the strong forces exerted by high-shear mixers. With longer mixing times, more particles are subjected to shearing.

It is also worth noting that batches with longer mixing times exhibited fewer agglomerates on the surfaces of the lactose particles in comparison to those with shorter mixing times. This is interesting considering that the FPF decreased with longer mixing times and that the impact on the pre-separator and throat increased. However, it is challenging to determine whether the agglomerates are budesonide, fines, or something else. Furthermore, due to differences in resolution among the images, drawing definitive conclusions is difficult. Additionally, it is important to acknowledge that the samples only represent a very small portion of the entire sample.

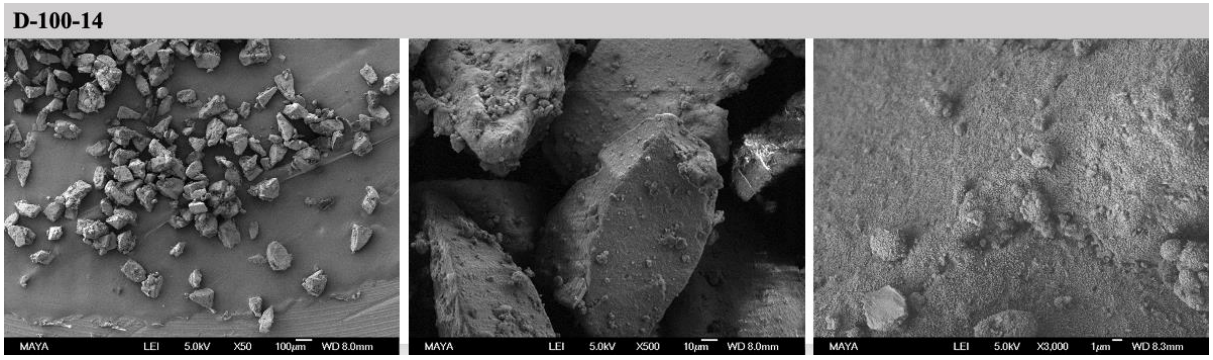

Figure 39: SEM images of batch D-100-14. The images were taken at an acceleration voltage of 5,0 kV, a working distance of 8, 8, and 8,3 mm, and a magnification of X50, X500, and X3000 respectively. The detector used was the lower secondary electron detector (LEI).

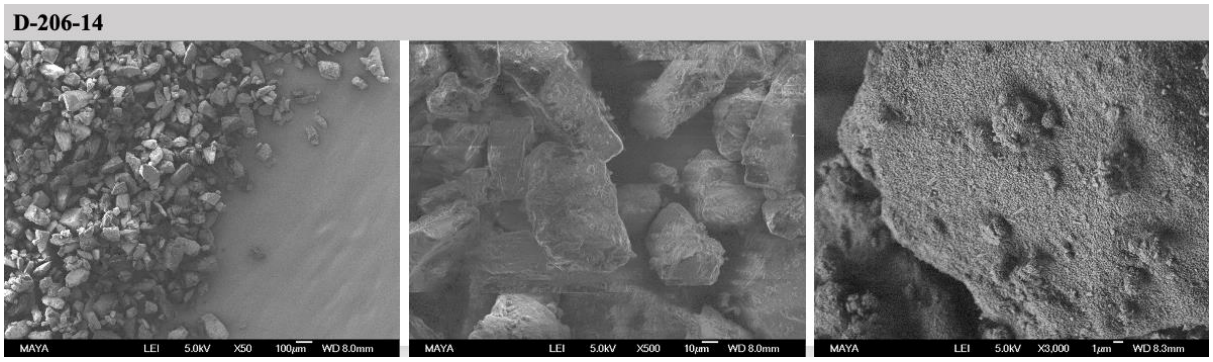

Figure 40: SEM images of batch D-206-14. The images were taken at an acceleration voltage of 5,0 kV, a working distance of 8, 8, and 8,3 mm, and a magnification of X50, X500, and X3000 respectively. The detector used was the lower secondary electron detector (LEI).

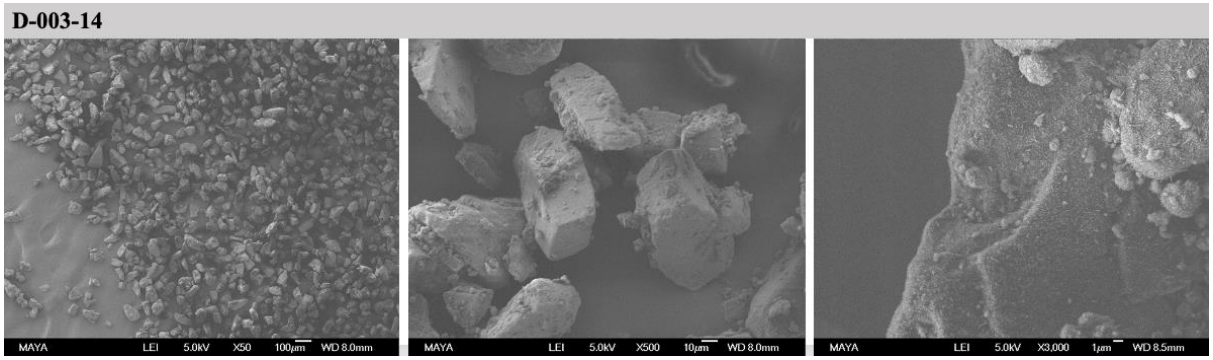

Figure 41: SEM images of batch D-003-14. The images were taken at an acceleration voltage of 5,0 kV, a working distance of 8, 8, and 8,5 mm, and a magnification of X50, X500, and X3000 respectively. The detector used was the lower secondary electron detector (LEI).

4.7 Comparison of Diosna and Turbula batches – mixing energy

To further compare the results between the Diosna and Turbula batches, the mixing energy was used. The mixing energy was calculated according to equations (5) and (6), see section 2.3.

4.7.1 FPF and mixing energy

There have been uncertainties regarding the mixing energy equation and whether the mass of the carrier should be included. To investigate this, the FPF was plotted against the mixing energy, but excluding the mass of the carrier from the mixing energy equation (see Figure 42). Significant differences were observed between the three carriers, suggesting that the mass of the carrier does have an impact on the mixing energy equation and should therefore be considered. Furthermore, when examining LH100, it is evident that the FPF decreases rapidly. If, for example, the mixing speed or time were to be increased, the FPF would approach zero rapidly.

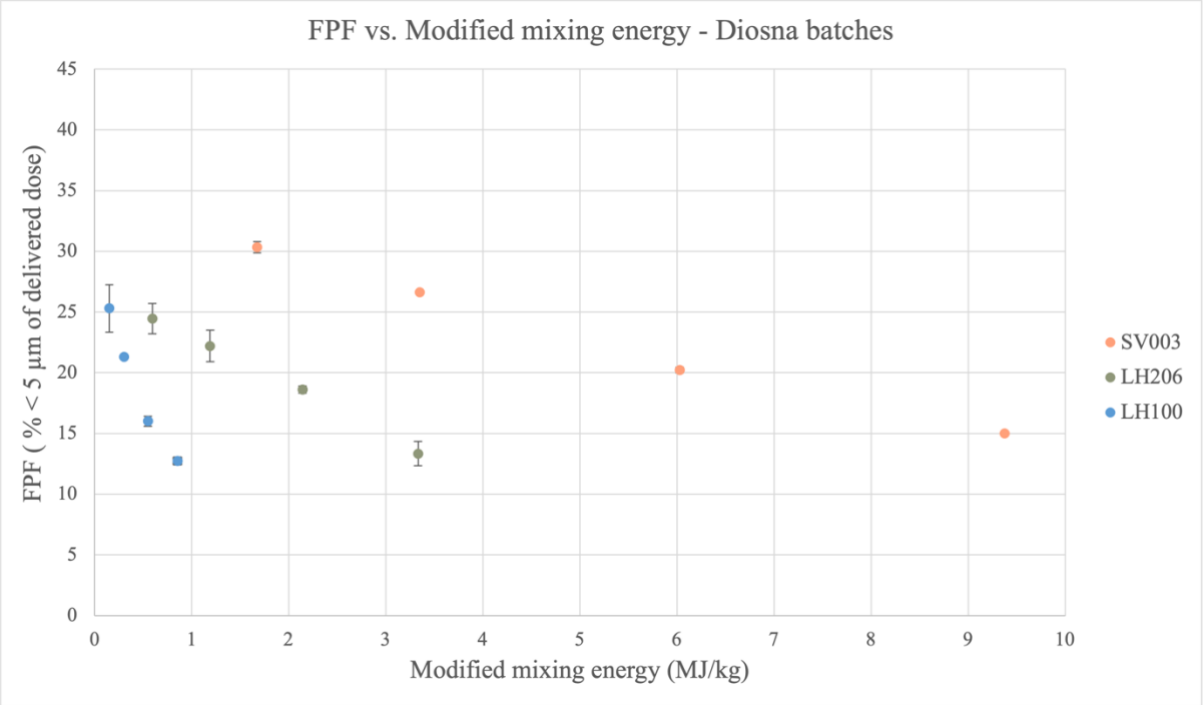

Figure 42: FPF plotted against modified mixing energy for the Diosna batches. The modified mixing energy refers to the mixing energy equation but with the mass of the carrier excluded. The error bars represent the standard deviation.

To see how FPF changes with the mixing energy, the FPF was plotted against the mixing energy, including the mass of the carrier, see Figure 43. For all Diosna batches, the FPF decreased with increased mixing energy. As can be seen in Figure 43, despite similar mixing energies, there is a difference in FPF, especially for the batches with SV003 as the carrier. However, the hypothesis was that batches with similar mixing energies would obtain similar FPF. LH100 and LH206-batches seem to be more similar in FPF compared to the SV003-batches. Furthermore, the slopes of the equation for the linear regression for the three lactose carriers are similar, indicating a correlation.

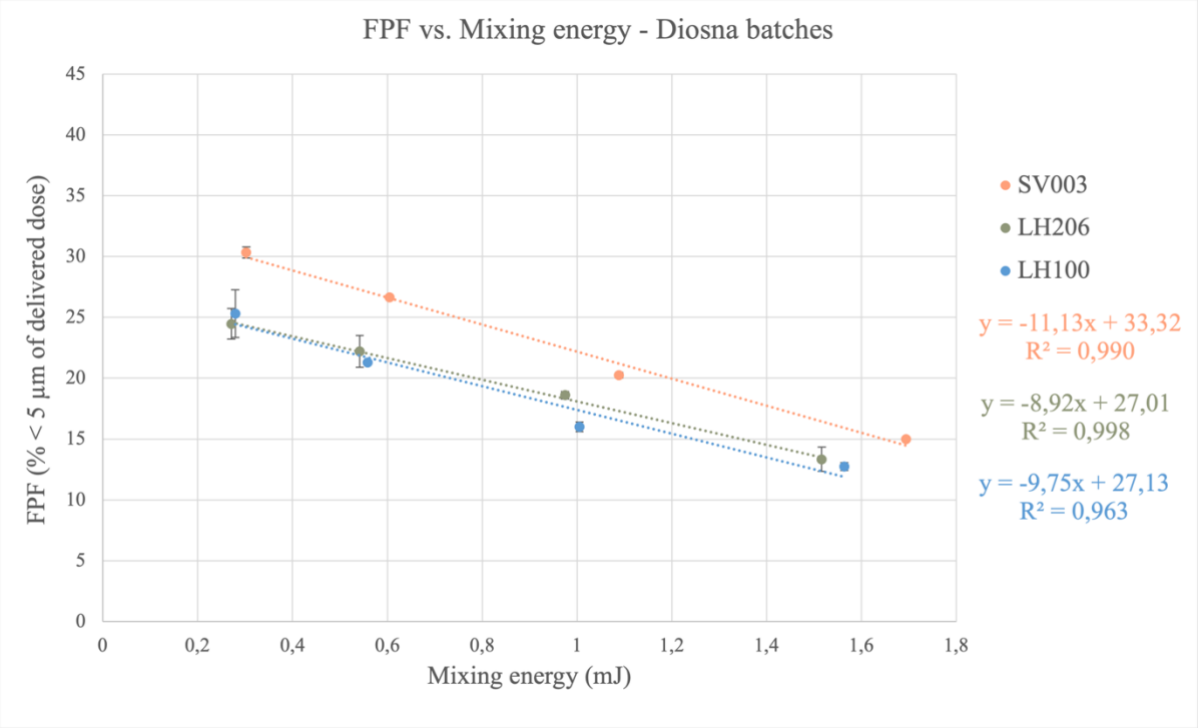

Figure 43: FPF plotted against the mixing energy for the Diosna batches. The linear regression and R^2 values are presented for each carrier (blue – LH100, green – LH206, and orange – SV003). The error bars represent the standard deviation.

Due to the limited number of mixing times for the Turbula batches, it is challenging to perform a reliable linear regression. However, as shown in Figure 44, there is no clear correlation between the FPF and mixing energy. There appears to be a correlation between batches using LH100 and LH206 as carriers, though it is not linear. For SV003, it is uncertain if this carrier aligns with the hypothesis. Notably, very low mixing energies were used for SV003, making it interesting to investigate whether higher mixing energies would impact the correlation. This suggests that the mixing energy applies to the Turbula mixer, however, in a different way than the Diosna mixer.

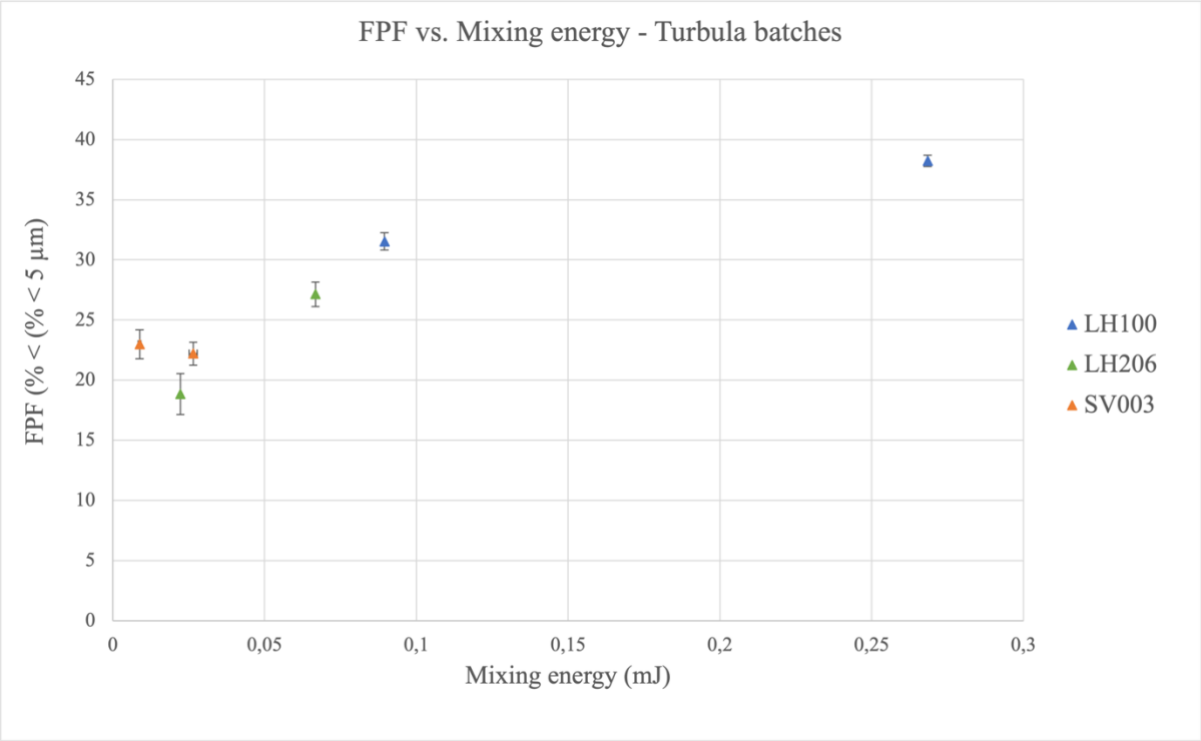

Figure 44: FPF plotted against the mixing energy for the Turbula batches. The error bars represent the standard deviation.

4.7.2 Fraction deposited in pre-separator and throat and mixing energy

To further compare the mixers based on mixing energy, the fraction deposited in the pre-separator and throat for the Diosna batches was plotted against the mixing energy, see Figure 45. There is an increase in the fraction of budesonide deposited with increased mixing energy. Furthermore, there seems to be a correlation between the fraction deposited in the upper parts of the NGI (pre-separator and throat) and mixing energy for all Diosna batches. When examining the fitted linear equation for batches with LH100 and LH206 as carriers, the equations are similar. However, for batches with SV003 as the carrier, the values are slightly lower compared to those with LH100 and LH206. This difference could be attributed to the higher delivered dose observed in the SV003 batches.

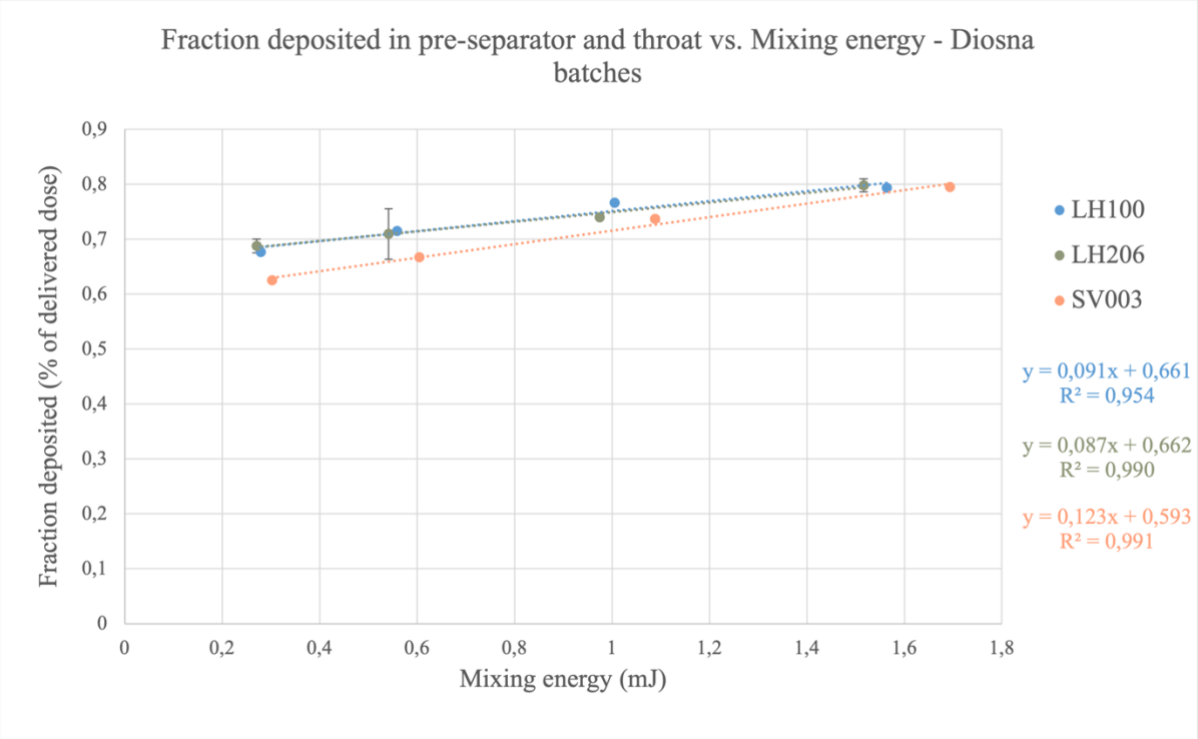

Figure 45: Fraction budesonide deposited in the pre-separator and throat (defined as % of delivered dose) plotted against the mixing energy for the Diosna batches. The linear regression and R^2 values are presented for each carrier (blue – LH100, green – LH206, and orange – SV003). The error bars represent the standard deviation.

To further compare the Diosna and Turbula mixer based on the fraction of budesonide deposited in the pre-separator and throat, Turbula and Diosna batches for each carrier were plotted, see Figure 46. As mentioned previously, for the Diosna batches, the fraction of budesonide deposited in the pre-separator and throat increased with increased mixing energy. For the Turbula batches, however, the opposite trend was observed for batches with LH100 and LH206 as the carriers. The same trends have been observed by Thalberg et. Al and potential explanations are that, in the Turbula mixer, de-agglomeration of the API improves with increased mixing time. For the Diosna batches, the API particles are incorporated into the carrier surfaces because of the forces generated during high-shear mixing, leading to a reduction in the fraction of budesonide available for dispersion. [23]

For batches with SV003 as the carrier, the fraction deposited in the pre-separator and throat increased with increased mixing energy for both Diosna and Turbula batches.

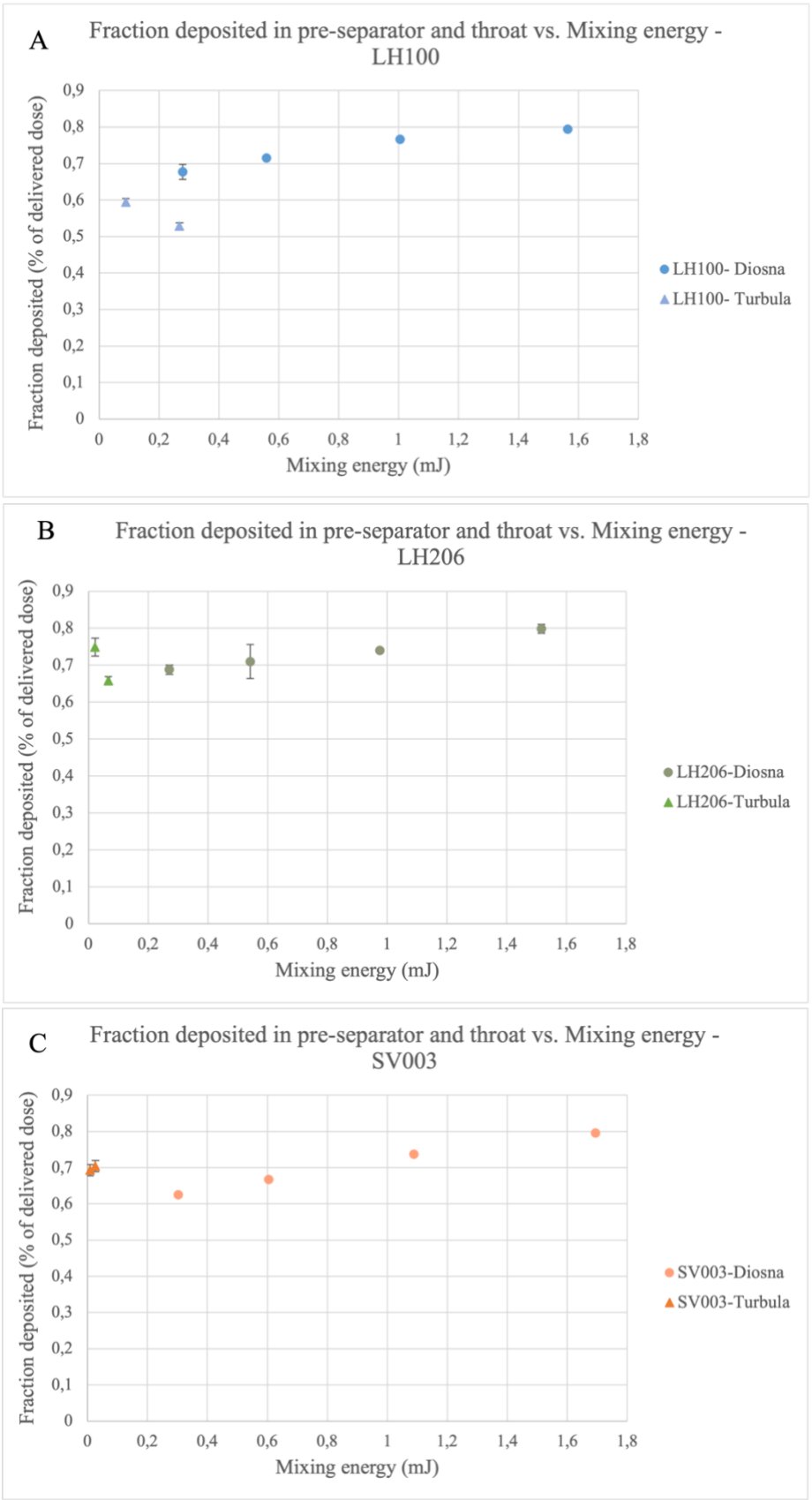

Figure 46: Fraction of budesonide deposited in the pre-separator and throat for the Diosna and Turbula batches (A – for batches with LH100, B – for batches with LH206, and C – for batches with SV003). The error bars represent the standard deviation.

5. Conclusion

The project aimed to investigate the effect of using different sizes of lactose carrier particles on capsule DPI performance, as well as the effect of using different mixers (Diosna and Turbula), mixing time, and speed.

For the Diosna batches, the FPF decreased with increased mixing time, and the opposite trend was observed for the Turbula batches. The highest FPF among all the batches was obtained for batch T-100-60. The Diosna batches with SV003 as the carrier performed significantly better in FPF, and FPD, and retained a more stable delivered dose compared to the batches with LH100 and LH206 as the carriers. Furthermore, these batches had the least capsule retention, indicating that the powder more efficiently escaped the capsule upon inhalation. Moreover, these batches obtained the lowest impact on the pre-separator and throat, which could potentially indicate that budesonide was more evenly spread out on SV003 or that the adhesive forces were optimal. The batches that performed the worst in FPF among the Diosna batches were the ones with LH100 as the carrier. However, LH100 and LH206 performed similarly in most of the other analyses.

Among the batches that were produced in the Turbula mixer, batches with LH100 as the carrier obtained the highest FPF and FPD compared to the batches with LH206 and SV003 as carriers. The impact on the pre-separator and throat was also the lowest for batches with LH100 and highest for T-206-20 and T-003-60. Here, it seems that a larger lactose carrier particle destroys budesonide aggregates better, which also aligns with the homogeneity measurements as the relative standard deviation increased with a decreased size of the lactose particle. The capsule retention seems to decrease with increased mixing time which could be explained by the increase in bulk density with longer mixing times, thus, increased flowability.

A higher delivered dose was obtained for batches with SV003 as the carrier, independently of the mixer used. This could potentially be explained by the fact that the weight of SV003 is so small that a larger portion can escape the capsule upon inhalation and thus enter the NGI. Furthermore, the capsule retention was considerably much lower for batches produced in the Diosna mixer, especially with longer mixing times. This could be explained by the fact that the more aggressive mixing process in high-shear mixers results in higher mixing forces on the particles, which causes the API to be pushed harder into the lactose carriers, thus improving capsule retention.

When comparing the FPF against the mixing energy it seems like the Diosna batches benefit from smaller mixing energies. This could be achieved either by lowering the mixing speed or lowering the mixing time. Furthermore, when comparing the mixers based on the mixing energy, it is evident that the mixing energy theory applies to both the Diosna mixer and the Turbula mixer. However, the mixing energy seems to affect the performances of the formulations differently depending on the type of mixer. It is also concluded that the mass of the carrier particle should be included in the mixing energy equation.

The effect of different mixing times highly affected the surfaces of the lactose particles, according to SEM. Needle-like particles were visible on the surfaces of the lactose particles on

batches produced in the Diosna mixer that had been mixed for 14 minutes, compared to batches produced for 2,5 minutes. This is probably due to the strong forces exerted on the particles in high-shear mixers which causes the particles to shear.

During manufacturing, electrostatic effects of the formulation were observed to a very small extent and were not considered a problem during handling. For batches produced in the Diosna mixer, the amount of powder stuck on the walls increased with smaller lactose carrier particles. All batches were considered homogenous, with an RSD < 5%.

For all batches, the bulk density increased compared to the pure carriers, indicating that budesonide had been filling up cavities on the lactose, as well as improving the flowability of the powder. Furthermore, it was established that for the Diosna batches, a decrease in bulk density was observed after 2 months of storage. The same was observed for the Turbula batches, with exceptions for batches with LH100 as the carrier, where an increase in bulk density was observed after 2 months of storage. This increase in bulk density could be explained by that the powder has had time to relax, thereby eliminating electrostatic effects, or that the powder has absorbed moisture from the surroundings.

5.1 Future Directions

To further investigate the effect of lactose carrier particle size it would be interesting to examine:

- If a higher FPF is obtained when produced in a high-shear mixer and using a lactose carrier with a particle size distribution smaller than Respitose® SV003
- If a higher FPF is obtained when produced in a low-shear mixer and using a lactose carrier with a particle size distribution larger than Lactohale® 100
- The effect of using another type of inhaler but the same lactose carrier particles used in this degree project

Additionally, it would be interesting to investigate how longer mixing times than 60 minutes in the Turbula mixer affect the dispersion of the formulation, as well as if there is a maximum in FPF.

7. References

1. Ali M. CHAPTER 9 - Pulmonary Drug Delivery. In: Kulkarni VS, editor. Handbook of Non-Invasive Drug Delivery Systems. Boston: William Andrew Publishing; 2010. p. 209-46.

2. Sanders M. Inhalation therapy: an historical review. Primary Care Respiratory Journal. 2007;16:71-81.

3. Aulton ME, editor. Aulton's Pharmaceutics The Design and Manufacture of Medicines. 3 ed: Churchill Livingstone Elsevier; 2007.

4. Moshe Haddad SS. Physiology, Lung: StatPearls Publishing; 2023 [Available from: https://www.ncbi.nlm.nih.gov/books/NBK545177/.

5. Telko MJ HA. Dry powder inhaler formulation. Respir Care. 2005;50(9):1209-27.

6. Newman SP. AEROSOLS. In: Laurent GJ, Shapiro SD, editors. Encyclopedia of Respiratory Medicine. Oxford: Academic Press; 2006. p. 58-64.

7. Bai S, Gupta V, Ahsan F. Inhalable lactose-based dry powder formulations of low molecular weight heparin. J Aerosol Med Pulm Drug Deliv. 2010;23(2):97-104.

8. Thalberg K. Formulation development of adhesive mixtures for inhalation - A multi-factorial optimization challenge: Part 1. Inhalation. 2022.

9. Nguyen DT, Rasmuson A, Niklasson Björn I, Thalberg K. Mechanistic time scales in adhesive mixing investigated by dry particle sizing. European journal of pharmaceutical sciences : official journal of the European Federation for Pharmaceutical Sciences. 2015;69:19-25.

10. Kaialy W. On the effects of blending, physicochemical properties, and their interactions on the performance of carrier-based dry powders for inhalation — A review. Advances in Colloid and Interface Science. 2016;235:70-89.

11. Peng T, Lin S, Niu B, Wang X, Huang Y, Zhang X, et al. Influence of physical properties of carrier on the performance of dry powder inhalers. Acta Pharmaceutica Sinica B. 2016;6(4):308-18.

12. Hopke PK, Casuccio GS. Chapter 6 - Scanning Electron Microscopy. In: Hopke PK, editor. Data Handling in Science and Technology. 7: Elsevier; 1991. p. 149-212.

13. Marple VA, Roberts DL, Romay FJ, Miller NC, Truman KG, Van Oort M, et al. Next generation pharmaceutical impactor (a new impactor for pharmaceutical inhaler testing). Part I: Design. J Aerosol Med. 2003;16(3):283-99.

14. Scientific C. Driving Results in Inhaler Testing. 2021. p. 82-6.

15. Newman SP. Fine Particle Fraction: The Good and the Bad. J Aerosol Med Pulm Drug Deliv. 2022;35(1):2-10.

16. Thalberg K, Berg E, Fransson M. Modeling dispersion of dry powders for inhalation. The concepts of total fines, cohesive energy and interaction parameters. International Journal of Pharmaceutics. 2012;427(2):224-33.

17. Ltd. MI. SprayTec User Manual. 2007.

18. Rudén J. Powder mechanics and dispersion properties of adhesive mixtures for dry powder inhalers Conceptualized as a blend state model [Dissertation]: Uppsala University; 2021.

19. Chaurasiya B, Zhao YY. Dry Powder for Pulmonary Delivery: A Comprehensive Review. Pharmaceutics. 2020;13(1).

20. Flament M-P, Leterme P, Gayot A. The influence of carrier roughness on adhesion, content uniformity and the in vitro deposition of terbutaline sulphate from dry powder inhalers. International Journal of Pharmaceutics. 2004;275(1):201-9.

21. Kaialy W, Alhalaweh A, Velaga SP, Nokhodchi A. Influence of lactose carrier particle size on the aerosol performance of budesonide from a dry powder inhaler. Powder Technology. 2012;227:74-85.

22. Forss LL. Adhesive mixtures for dry powder inhalation. Uppsala, Sweden: Uppsala University; 2021.

23. Thalberg K, Ivarsson L, Svensson M, Elfman P, Ohlsson A, Stuckel J, Lyberg A-M. The effect of mixing on the dispersibility of adhesive mixtures for inhalation. Comparison of high shear and Turbula mixers. European Journal of Pharmaceutical Sciences. 2024;193:106679.

24. Spahn JE, Zhang F, Smyth HDC. Mixing of dry powders for inhalation: A review. International Journal of Pharmaceutics. 2022;619:121736.

25. Sebti T, Vanderbist F, Amighi K. Evaluation of the content homogeneity and dispersion properties of fluticasone DPI compositions. Journal of Drug Delivery Science and Technology. 2007;17(3):223-9.

26. Sachin Bhusari TC, Gaurav Shrangare, Pravin Wakte. Development and validation of UV-Visible spectrophotometer method for estimation of Budesonide in bulk and formulation. Journal of Pharma Research. 2018;7(12).

27. Shur J, Saluja B, Lee S, Tibbatts J, Price R. Effect of Device Design and Formulation on the In Vitro Comparability for Multi-Unit Dose Dry Powder Inhalers. Aaps j. 2015;17(5):1105-16.

8. Appendices

Appendix A – Formulation composition

Formulation composition for batches using the Diosna mixer.

Batch	Budesonide (g)	Lactose (g)	Total (g)	Budesonide (%)
D-100	5,0190	245,8300	250,8490	2,0
D-206	5,0168	245,8200	250,8368	2,0
D-003	5,0113	245,1500	250,1613	2,0

Formulation composition for batches using the Turbula mixer.

Batch	Budesonide (g)	Lactose (g)	Total (g)	Budesonide (%)
T-100-20	1,6145	78,38	79,9945	2,0
T-100-60	1,6045	78,43	80,0345	2,0
T-206-20	1,6075	78,39	79,9975	2,0
T-206-60	1,6034	78,44	80,0434	2,0
T-003-20	1,5979	78,44	80,0379	2,0
T-003-60	1,6078	78,42	80,0278	2,0

Appendix B – NGI data from Diosna batches

Batches D-100-2,5, D-100-5, D-100-9, and D-100-14

Batch	D-100-2,5			D-100-5		
Flow rate (l/min)		43			43	
No of inhalers		3			3	
No of doses per inhaler		6			6	
	Mean	SD	RSD%	Mean	SD	RSD%
Total dose (µg/dose)	469,10	2,80	0,60	460,80	3,23	0,70
Delivered dose (µg/dose)	426,40	5,97	1,40	411,50	6,17	1,50
Throat (µg/dose)	52,65	3,31	6,28	43,77	2,03	4,63
Pre-separator (µg/dose)	236,18	11,26	4,78	250,30	3,30	1,32
Capsule retention (% of total)	14,10	1,18	8,40	10,70	0,88	8,20
Fine particle dose (µg/dose < 5 µm)	107,70	6,89	6,40	87,80	1,76	2,00
Fine particle fraction (% < 5 µm of DD)	25,30	1,97	7,80	21,30	0,09	0,40
MMAD (µm)	2,56	0,07	2,72	2,93	0,03	1,08
R-value		1,00			1,00	
Batch	D-100-9			D-100-14		
Flow rate (l/min)		43			43	
No of inhalers		3			3	
No of doses per inhaler		6			6	
	Mean	SD	RSD%	Mean	SD	RSD%
Total dose (µg/dose)	512,9	3,08	0,60	522,2	3,66	0,70
Delivered dose (µg/dose)	465,5	6,52	1,40	477,6	3,82	0,80
Throat (µg/dose)	54,4	4,65	8,54	50,1	3,23	6,46
Pre-separator (µg/dose)	302,3	8,63	2,85	329,1	4,97	1,51
Capsule retention (% of total)	9,2	1,40	15,20	8,5	0,53	6,20
Fine particle dose (µg/dose < 5 µm)	74,5	1,94	2,60	60,7	1,52	2,50
Fine particle fraction (% < 5 µm of DD)	16,0	0,40	2,50	12,7	0,32	2,50
MMAD (µm)	3,51	0,09	2,70	4,09	0,06	1,36
R-value		1,00			1,00	

Batches D-206-2,5, D-206-5, D-206-9, and D-206-14

Batch	D-206-2,5			D-206-5		
Flow rate (l/min)		43			43	
No of inhalers		3			3	
No of doses per inhaler		6			6	
	Mean	**SD**	**RSD%**	**Mean**	**SD**	**RSD%**
Total dose (µg/dose)	467,60	12,63	2,70	508,80	6,61	1,30
Delivered dose (µg/dose)	393,90	9,85	2,50	453,70	11,80	2,60
Throat (µg/dose)	52,20	3,76	7,20	56,75	3,64	6,41
Pre-separator (µg/dose)	218,78	4,83	2,21	264,99	11,54	4,36
Capsule retention (% of total)	15,80	0,21	1,30	10,80	1,20	11,10
Fine particle dose (µg/dose < 5 µm)	96,40	5,69	5,90	100,70	3,32	3,30
Fine particle fraction (% < 5 µm of DD)	24,50	1,25	5,10	22,20	1,29	5,80
MMAD (µm)	2,71	0,05	1,96	2,99	0,04	1,50
R-value		1,00			1,00	
Batch	**D-206-9**			**D-206-14**		
Flow rate (l/min)		**43**			**43**	
No of inhalers		3			3	
No of doses per inhaler		6			6	
	Mean	**SD**	**RSD%**	**Mean**	**SD**	**RSD%**
Total dose (µg/dose)	509,10	9,16	1,80	523,20	4,19	0,80
Delivered dose (µg/dose)	466,60	6,07	1,30	480,50	3,84	0,80
Throat (µg/dose)	49,24	1,79	3,64	54,41	0,80	1,47
Pre-separator (µg/dose)	295,98	7,02	2,37	329,08	3,94	1,20
Capsule retention (% of total)	8,40	0,65	7,70	8,20	0,86	10,50
Fine particle dose (µg/dose < 5 µm)	86,90	0,26	0,30	64,10	4,94	7,70
Fine particle fraction (% < 5 µm of DD)	18,60	0,28	1,50	13,30	0,96	7,20
MMAD (µm)	3,47	0,02	0,64	3,81	0,05	1,32
R-value		1,00			1,00	

Batches D-003-2,5, D-003-5, D-003-9, and D-003-14

Batch	D-003-2,5			D-003-5		
Flow rate (l/min)		43			43	
No of inhalers		3			3	
No of doses per inhaler		6			6	
	Mean	SD	RSD%	Mean	SD	RSD%
Total dose (µg/dose)	521,70	2,09	0,40	525,00	3,68	0,70
Delivered dose (µg/dose)	481,70	3,85	0,80	481,30	2,89	0,60
Throat (µg/dose)	48,17	1,78	3,69	48,73	2,40	4,92
Pre-separator (µg/dose)	252,97	4,12	1,63	272,57	3,63	1,33
Capsule retention (% of total)	7,70	0,61	7,90	8,30	1,18	14,20
Fine particle dose (µg/dose < 5 µm)	146,10	1,02	0,70	128,20	0,64	0,50
Fine particle fraction (% < 5 µm of DD)	30,30	0,45	1,50	26,60	0,11	0,40
MMAD (µm)	2,71	0,04	1,64	2,87	0,03	1,05
R-value		1,00			1,00	
Batch	D-003-9			D-003-14		
Flow rate (l/min)		43			43	
No of inhalers		3			3	
No of doses per inhaler		6			6	
	Mean	SD	RSD%	Mean	SD	RSD%
Total dose (µg/dose)	532,80	10,66	2,00	537,10	8,06	1,50
Delivered dose (µg/dose)	490,70	5,40	1,10	500,40	6,51	1,30
Throat (µg/dose)	55,87	3,02	5,40	61,50	8,62	14,02
Pre-separator (µg/dose)	305,70	3,76	1,23	336,51	10,03	2,98
Capsule retention (% of total)	7,90	1,30	16,40	6,80	0,58	8,60
Fine particle dose (µg/dose < 5 µm)	99,40	2,09	2,10	75,10	0,83	1,10
Fine particle fraction (% < 5 µm of DD)	20,20	0,22	1,10	15,00	0,03	0,20
MMAD (µm)	3,14	0,06	2,02	3,39	0,01	0,40
R-value		1,00			1,00	

Appendix C – NGI data from Turbula batches

Batches T-100-20 and T-100-60

Batch	T-100-20			T-100-60		
Flow rate (l/min)		43			43	
No of inhalers		3			3	
No of doses per inhaler		6			6	
	Mean	SD	RSD%	Mean	SD	RSD%
Total dose (µg/dose)	475,50	15,69	3,30	470,50	9,88	2,10
Delivered dose (µg/dose)	388,20	9,32	2,40	409,40	3,28	0,80
Throat (µg/dose)	46,36	3,67	7,91	40,13	1,61	4,00
Pre-separator (µg/dose)	184,23	1,81	0,99	176,20	1,85	1,05
Capsule retention (% of total)	15,10	1,48	9,80	12,90	2,46	19,10
Fine particle dose (µg/dose < 5 µm)	122,50	4,90	4,00	156,60	3,29	2,10
Fine particle fraction (% < 5 µm of DD)	31,60	0,73	2,30	38,30	0,50	1,30
MMAD (µm)	2,83	0,02	0,69	2,71	0,01	0,26
R-value		1,00			1,00	

Batches T-206-20 and T-206-60

Batch	T-206-20			T-206-60		
Flow rate (l/min)		43			43	
No of inhalers		3			3	
No of doses per inhaler		6			6	
	Mean	SD	RSD%	Mean	SD	RSD%
Total dose (µg/dose)	483,10	20,29	4,20	462,50	19,43	4,20
Delivered dose (µg/dose)	404,60	8,09	2,00	389,50	21,03	5,40
Throat (µg/dose)	79,43	17,55	22,10	59,13	4,63	7,83
Pre-separator (µg/dose)	223,50	9,36	4,19	197,27	13,22	6,70
Capsule retention (% of total)	16,20	1,96	12,10	15,80	1,07	6,80
Fine particle dose (µg/dose < 5 µm)	76,30	7,94	10,40	105,50	3,48	3,30
Fine particle fraction (% < 5 µm of DD)	18,80	1,71	9,10	27,10	1,00	3,70
MMAD (µm)	2,98	0,06	1,91	2,83	0,03	0,90
R-value		1,00			1,00	

Batches T-003-20 and T-003-60

Batch	T-003-20			T-003-60		
Flow rate (l/min)		43			43	
No of inhalers		3			3	
No of doses per inhaler		6			6	
	Mean	SD	RSD%	Mean	SD	RSD%
Total dose (µg/dose)	486,50	10,22	2,10	485,40	18,45	3,80
Delivered dose (µg/dose)	417,40	10,02	2,40	415,60	19,12	4,60
Throat (µg/dose)	65,67	2,01	3,07	71,10	4,23	5,95
Pre-separator (µg/dose)	223,67	7,85	3,51	221,77	18,33	8,27
Capsule retention (% of total)	14,20	1,01	7,10	14,40	0,75	5,20
Fine particle dose (µg/dose < 5 µm)	96,00	5,28	5,50	92,10	3,96	4,30
Fine particle fraction (% < 5 µm of DD)	23,00	1,20	5,20	22,20	0,98	4,40
MMAD (µm)	3,01	0,02	0,73	3,07	0,09	2,94
R-value		1,00			1,00	